Master Thesis

Czech Technical University in Prague

F3

Faculty of Electrical Engineering
Department of Electromagnetic Field

Broadband Extraction of Sample Permittivity from Microwave Planar Passive Devices Measurements

Bc. Petr Kůrka

Supervisors:
Ing. Ladislav Oppl, Ph.D.
Ing. Michal Cifra, Ph.D.
Ing. Daniel Havelka, Ph.D.
May 2022

ZADÁNÍ DIPLOMOVÉ PRÁCE

I. OSOBNÍ A STUDIJNÍ ÚDAJE

Příjmení: **Kůrka** Jméno: **Petr** Osobní číslo: **468799**

Fakulta/ústav: **Fakulta elektrotechnická**

Zadávající katedra/ústav: **Katedra mikroelektroniky**

Studijní program: **Elektronika a komunikace**

Specializace: **Elektronika**

II. ÚDAJE K DIPLOMOVÉ PRÁCI

Název diplomové práce:

Širokopásmová extrakce permitivity vzorků z měření mikrovlnných pasivních planárních zařízení

Název diplomové práce anglicky:

Broadband Extraction of Sample Permittivity from Microwave Planar Passive Devices Measurements

Pokyny pro vypracování:

1. Nastudujte literaturu o metodách širokopásmové extrakce komplexní permitivity materiálů se zaměřením na planární vedení, konkrétně koplanární vlnovod.
2. Implementujte metodu pro semi/analytickou extrakci s cílem získat spektra komplexní permitivity z naměřených frekvenčně závislých S-parametrů.
3. Změřte S-parametry koplanárních vedení s vybranými vzorky do 50 GHz.
4. Metodu pro extrakci permitivity ověřte na získaných datech. Data porovnejte s referenčními údaji z literatury. Zhodnoťte dosažené výsledky.

Seznam doporučené literatury:

1. Booth et al., "Quantitative Permittivity Measurements of Nanoliter Liquid Volumes in Microfluidic Channels to 40 GHz." IEEE Trans. on IM 59, no. 12 (December 2010): 3279–88. https://doi.org/10.1109/TIM.2010.2047141.
2. Liu et al., "Hybrid Characterization of Nanolitre Dielectric Fluids in a Single Microfluidic Channel Up to 110 GHz." IEEE Trans. on MTT 65, no. 12 (2017): 5063–73. https://doi.org/10.1109/TMTT.2017.2731950.
3. Bao et al. "A General Line–Line Method for Dielectric Material Characterization Using Conductors With the Same Cross-Sectional Geometry." IEEE MWCL 28, no. 4 (April 2018): 356–58. https://doi.org/10.1109/LMWC.2018.2809041.

Jméno a pracoviště vedoucí(ho) diplomové práce:

Ing. Ladislav Oppl, Ph.D.   katedra elektromagnetického pole   FEL

Jméno a pracoviště druhé(ho) vedoucí(ho) nebo konzultanta(ky) diplomové práce:

Datum zadání diplomové práce: **16.02.2022** Termín odevzdání diplomové práce: **20.05.2022**

Platnost zadání diplomové práce: **19.02.2024**

_____ _____ _____
Ing. Ladislav Oppl, Ph.D.   prof. Ing. Pavel Hazdra, CSc.   prof. Mgr. Petr Páta, Ph.D.
podpis vedoucí(ho) práce   podpis vedoucí(ho) ústavu/katedry   podpis děkana(ky)

III. PŘEVZETÍ ZADÁNÍ

Diplomant bere na vědomí, že je povinen vypracovat diplomovou práci samostatně, bez cizí pomoci, s výjimkou poskytnutých konzultací.
Seznam použité literatury, jiných pramenů a jmen konzultantů je třeba uvést v diplomové práci.

_____ _____
.
Datum převzetí zadání   Podpis studenta

iv

Acknowledgements

Declaration

I declare that I elaborated this thesis on my own and that I mentioned all the information sources that have been used in accordance with the Guideline for adhering to ethical principles in the course of elaborating an academic final thesis.

In Prague, 19. May 2022

Abstract

Knowledge of the electromagnetic properties of biomolecules is important for the understanding of the interaction of electric fields with biosystems and for the development of novel biomedical diagnostic and therapeutic methods. However, developments in this field are hampered by the large sample volumes required for permittivity extraction.

The aim of this work is to propose a novel method for obtaining a broadband complex permittivity based on a conductor–backed coplanar waveguide. The main advantage of this method is the ability to measure the dielectric properties of extremely small sample volumes (in the order of µL), approximately 20 times smaller than with commercially available methods.

The method is then tested in real life on measured S–parameters of an aqueous solution of selected biomolecules (L-alanine and L-cysteine) with different concentrations in the frequency band 1.5 – 50 GHz.

The extracted permittivity is then compared with the permittivity values obtained by another independent reference method.

Keywords: complex permittivity; broadband; S–parameters; coplanar waveguide; biomolecules; transmission line; liquid samples

Supervisors:

Ing. Ladislav Oppl, Ph.D.[1]
Ing. Michal Cifra, Ph.D.[2]
Ing. Daniel Havelka, Ph.D.[2]

[1]Department of Electromagnetic Field
[2]Institute of Photonics and Electronics
 of the Czech Academy of Sciences

Abstrakt

Znalost elektromagnetických vlastností biomolekul je důležitá pro pochopení interakce elektrických polí s biosystémy a pro vývoj nových biomedicínských diagnostických a terapeutických metod. Rozvoji v této oblasti však brání velké objemy vzorků potřebné pro extrakci permitivity.

Cílem této práce je navrhnout novou metodu pro získání širokopásmové komplexní permitivity založené na zeměném koplanárním vlnovodu. Hlavní výhodou této metody je možnost měřit dielektrické vlastnosti extrémně malých objemů vzorků (řádově µL), přibližně 20-krát menších než u komerčně dostupných metod.

Metoda je následně testována v praxi na naměřených S-parametrech roztoku vody a vybraných biomolekul (L-alanin a L-cystein) o různých koncentracích ve frekvenčním pásmu 1,5 – 50 GHz.

Extrahovaná permitivita je poté porovnána s hodnotami permitivity získanými jinou nezávislou referenční metodou.

Klíčová slova: komplexní permitivita; širokopásmové; S–parametry; koplanární vlnovod; biomolekuly; přenosové vedení; kapalné vzorky

Překlad názvu: Širokopásmová extrakce permitivity vzorků z měření mikrovlnných pasivních planárních zařízení

Contents

Figures

Tables

Chapter 1

Introduction

Knowledge of the electromagnetic properties of biomolecules is important for the understanding of the interaction of electric fields with biosystems and for the development of novel biomedical diagnostic and therapeutic methods. Electromagnetic fields in radio and microwave frequency bands interact with biological systems mainly through the electrical component of the field [4]. Determining the permittivity of biomolecules is therefore crucial for determining the electromagnetic properties of proteins, cells and the whole living organisms. However, developments in this field are hampered by the large sample volumes associated with permittivity extraction.

The aim of this work is to propose a novel method for obtaining a broadband complex permittivity based on a conductor–backed coplanar waveguide (the transmission line design is based on [3]). The main advantage of this method is the ability to measure the dielectric properties of extremely small sample volumes (in the order of µL), approximately 20 times smaller than with commercially available methods [3]. This is a very desirable feature since purified protein samples can easily reach hundreds of EUR per mg.

The result of this work is an innovative method for extracting permittivity from the S–parameters. The method is then tested in real life on measured S–parameters of an aqueous solution of selected biomolecules (alanine and cysteine) with different concentrations in the frequency band 1.5 – 50 GHz. Alanine and cysteine are some of the most common proteinogenic amino acids, therefore, they are well described and readily available. For these reasons, alanine and cysteine were chosen as testing samples.

The extracted permittivity is then compared with the permittivity values obtained by another independent reference method.

1

Chapter 2

State of the Art

Here we review state of the art of technology for permittivity analysis in RF and MW bands focusing on techniques which employ vector network analyzers. The methods for extracting complex permittivity using a microwave vector network analyzer can be divided into four basic groups [5]:

- Coaxial probe

- Freespace

- Resonant cavity

- Transmission line

Now we briefly describe the advantages and disadvantages of each approach. Special attention will then be paid to the transmission line approach.

2.1 Coaxial Probe Techniques

Advantages [5]:

- Non-destructive for a large number of materials.

- Broad frequency range 0.2–50 GHz.

- Good for liquids or semisolids.

- Easy to use.

Disadvantages [5]:

- Need more sample volume.

- The sample must be homogeneous and isotropic.

- Problematic when measuring solids.

This is a well known technique of permittivity extraction. It is easy to use and works in a wide frequency range. It is not suitable for low-loss materials, magnetic materials, or where high precision is required [5].

2.2 Freespace Techniques

Advantages [5]:

- Non-contact and non-destructive for many materials. Suitable for non-contact measurement.

- Broad frequency range, to 325 GHz.

- It is possible to measure high temperature samples.

Disadvantages [5, 6]:

- More complex operation.

- Rather used for high frequencies from 100 GHz.

- Very large samples needed at low frequencies.

Technique suitable for sheet materials, powders, or liquids [5]. Its main problem is its price and its more complicated use.

2.3 Resonant Cavity Techniques

Advantages [5]:

- More accurate than broadband techniques.

- Ideal for low-loss materials.

- Small samples size.

Disadvantages [5]:

- Results at one frequency only.

- Not suitable for high loss materials.

- Complex post analysis.

This is the most accurate technique, especially for low-loss materials. The big limitation of this technique is that permittivity is extracted at only one frequency point and that the analysis can be complex.

2.4 Transmission Line Techniques

Advantages [3, 5]:

- A very affordable method based on coax or waveguide fixtures.

- Broad frequency range 0.1–110 GHz.

- Suitable for hard solid materials or liquids.

- It is possible to measure magnetic materials.

- Small samples size.

Disadvantages [5]:

- A precise shape of the sample is required (although this is not the case for our measuring structure [3]).

- Liquids, powders and gases must be contained.

- Large sample volume needed for low frequencies.

A very good techniques for investigating the effects of dissolved species in water. Provides information on understanding of the structure, molecular motions, and interactions in biological materials [6].

These techniques require the sample to be in close proximity to the measuring probe. The probe can be a transmission line section, waveguides, etc. [6]. The main advantage of these techniques is the ability to measure the dielectric properties of extremely small sample volumes. Where classical dielectric spectroscopy requires a large sample volume for high-frequency measurements, transmission line methods only need approximately 100 µL [3] or even less in order from 1–10 µL to nL [7, 8, 9].

Our goal is an affordable method for measuring small volumes of biomolecules dissolved in water, in wide frequency range. It is obvious that this direction of methods is the best for our work.

2.4.1 State of the Art of Transmission Line Techniques

The current body of scientific literature can be divided into two main directions, and so we we also divide this section. The first direction deals with measured transmission line quantities, such as sample capacitance (per length) and its contrast to some control for the purpose of biosensing. However, this direction does not result in broadband permittivity extraction. The aim of these methods is, for example, the detection of antibodies in cancer [10], label–free detection of changes in DNA [11], and so on.

The second direction results in a broadband permittivity extraction. Here the developments in this area are categorized on the basis of the way of obtaining the resulting complex permittivity [12, 13].

Simulator

This is a large family of methods that use a simulator for the final estimation of complex permittivity, see [14, 15, 7, 8, 16]. The principle of these methods is based on the fact that in a certain step, the least squares method minimizes the difference between the measured data (that is, S parameters, propagation coefficient γ, or distributed transmission line parameters) and the data from

the simulator. It is then possible to read the resulting values of complex permittivity from the simulator.

The advantage of these group of methods is a good accuracy [13]. The disadvantage is the high computational complexity. Obtaining complex permittivity by this method can be very time consuming.

■ Closed-Form Equations

This is a group of methods based on closed form equations. The complex permittivity in this case is directly expressed from the equations, see [17, 18, 19, 20, 21].

The advantage of these methods is the high speed of complex permittivity extraction. The disadvantage is lower accuracy compared to the complex permittivity obtained from simulator in the previous Section [13].

■ 2.4.2 Trace Method

Some methods from the previous Section 2.4.1 are specific in that they uses the so-called Trace equation (see Section 5, eq. (5.15)) to obtain permittivity. The advantage of these methods is that the Trace equation is based on differential measurements. This means that only the difference between measurements is used to obtain the permittivity and therefore we can neglect the influence of the whole transmission path from VNA (connection cables, transitions, and other imperfections leading to and from the sample), see [13, 22, 23]. The resulting permittivity from the measurement can then be obtained, for example, on the basis of a simulator [22].

Chapter 3

Interaction of Electromagnetic Fields with Dielectric Materials

Electromagnetic fields in radio and microwave frequency bands interact with biological systems mainly through the electrical component of the field [4]. For this reason, dielectric properties in this frequency band are key to characterizing and understanding the electromagnetic properties of biological systems.

3.1 Dielectrics in Time Dependent Fields

If we put a dielectric material into an electric field, its microscopic particles will begin to polarize in a way that reaches equilibrium with the acting electric field. If the rate of change of the electric field occurs much slower than the speed of motion of the microscopic particles, then the equilibrium between the dielectric material and the acting electric field can be reached at all times. Otherwise, there will be a dielectric displacement $D^*(t)$ which in the case of harmonic time-dependent fields can be written as:

$$D^*(t) = D_0 e^{i(\omega t - \delta(\omega))}, \tag{3.1}$$

where D_0 is constant, $\delta(\omega)$ is a phase difference with respect to the electric field, for a given frequency ω and t is time [6].

3.1.1 Complex Dielectric Permittivity

To describe the interaction of the dielectric material with the variable-frequency electric field, we need to introduce a complex, frequency–dependent dielectric permittivity $\epsilon^*(\omega)$ [6]:

$$\epsilon^*(\omega) = \frac{D_0}{\epsilon_0 E_0} e^{-i\delta(\omega)}, \tag{3.2}$$

where D_0 is the dielectric displacement, E_0 is the electric field intensity and ϵ_0 is the permittivity of vacuum. Usually, D_0 and E_0 are frequency dependent, so we can write:

$$D^*(\omega) = \epsilon_0 \epsilon^*(\omega) E^*(\omega). \tag{3.3}$$

After applying Euler's relations to the complex permittivity, we get the following:

$$\epsilon^*(\omega) = \epsilon'(\omega) - i\epsilon''(\omega), \tag{3.4}$$

where:

$$\epsilon'(\omega) = \frac{D_0(\omega)}{\epsilon_0 E_0(\omega)} \cos\left(\delta(\omega)\right) \tag{3.5}$$

$$\epsilon''(\omega) = \frac{D_0(\omega)}{\epsilon_0 E_0(\omega)} \sin\left(\delta(\omega)\right) \tag{3.6}$$

$$D_0(\omega) = \epsilon_0 E_0(\omega)\sqrt{\epsilon'^2(\omega) + \epsilon''^2(\omega)}. \tag{3.7}$$

Frequency dependent complex permittivity is particularly useful for describing lossy dielectric materials. The real part of Equation (3.4) then describes the electric polarizability and the imaginary part corresponds to energy losses.

▌ 3.2 Debye Model

The Debye model can be used to model and predict the complex permittivity of dielectric materials. To estimate the permittivity of a liquid sample consisting of only one type of molecule (e.g., pure water), a single–term Debye model can be used. To estimate the permittivity of a liquid sample consisting of two types of molecules (e.g., water and alanine), the two–term Debye model can be used. With extension of this logic, it is possible to describe samples consisting of three or more types of molecules.

▌ 3.2.1 Single–term Debye Model

In the event of a step change in the electric field, transients begin to occur in the dielectric. Microscopic particles of the dielectric material will reach a new equilibrium state after a characteristic period of time [6]. Lets consider a macroscopic relaxation function $\phi(t)$:

$$\phi(t) = e^{-\frac{t}{\tau}}, \tag{3.8}$$

where τ is the characteristic relaxation time of the dielectric material. In our specific case, the relaxation time of a spherical particle in a viscous medium can be written as [4]:

$$\tau = \frac{3V\eta}{k_B T}, \tag{3.9}$$

where V is the volume of amino acid, η is the dynamic viscosity of the solvent at temperature T and k_B is the Boltzmann constant. The frequency–dependent complex dielectric permittivity can be connected with the relaxation function through the following equation:

$$\frac{\epsilon^*(\omega) - \epsilon_h}{\epsilon_l - \epsilon_h} = \hat{L}\left[-\frac{d}{dt}\phi(t)\right], \tag{3.10}$$

where $\hat{L}$ represents the Laplace transform

$$\hat{L}[f(t)] = \int_0^\infty e^{-pt} f(t)dt, \ \ p = x + i\omega, \ \ x \to 0 \tag{3.11}$$

and ϵ_l is the low, ϵ_h is the high frequency limit of the permittivity for the given relaxation. Equation (3.10) is crucial because it states that it does not matter if the dielectric response is measured experimentally in the time or the frequency domain. In both ways, the obtained information will be equal [6].

By substituting Equation (3.8) into Equation (3.10) we get the famous Debye formula for the frequency–dependent dielectric permittivity:

$$\frac{\epsilon^*(\omega) - \epsilon_h}{\epsilon_l - \epsilon_h} = \frac{1}{1 + i\omega\tau}. \tag{3.12}$$

For real dielectrics, the equation can be written as:

$$\epsilon^*(\omega) = \epsilon_h + \frac{\epsilon_l - \epsilon_h}{1 + i\omega\tau} + \frac{\sigma_l}{i\epsilon_0\omega}, \tag{3.13}$$

where $\sigma_l / i\epsilon_0\omega$ is the added term of low frequency conductivity and σ_l is conductivity. The real part of the $\epsilon^*(\omega)$ function is equal to:

$$\epsilon'(\omega) = \epsilon_h + \frac{\epsilon_l - \epsilon_h}{1 + (\omega\tau)^2}. \tag{3.14}$$

The imaginary part is equal to:

$$\epsilon''(\omega) = \frac{\sigma_l}{\epsilon_0\omega} - \frac{\omega\tau(\epsilon_l - \epsilon_h)}{1 + (\omega\tau)^2}. \tag{3.15}$$
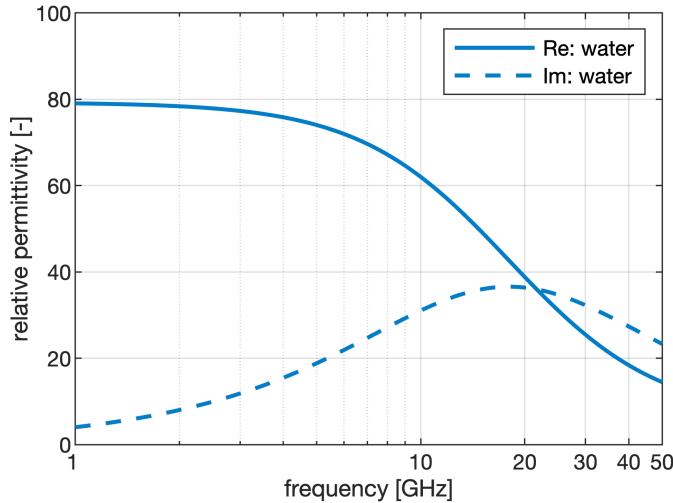
Figure 3.1: Single–term Debye model of complex water permittivity based on eq. 3.13. The values of the parameters are [1]: $\epsilon_h = 6.09$, $\epsilon_l = 79.27$, $\tau = 8.84$ (ps), $\sigma_l = 1.245 \cdot 10^{-4}$ (S/m).

In Figure 3.1, we can see a single–term Debye model of the complex permittivity of water. The real part of the complex permittivity is connected to the polarization of the microscopic particles of the dielectric material (water). At lower frequencies, the speed of motion of the microscopic particles is much higher than the rate of change of the electric field, so the real part of the permittivity remains constant. As the frequency rises, the microscopic particles losses their ability to follow the electric field and the real value of the permittivity starts to decline. The imaginary part of the permittivity is connected to the energy losses inside the dielectric material. As you can see, the steeper the slope of the real part of the permittivity, the higher the value of the imaginary part of the permittivity.

■ 3.2.2 Two–term Debye Model

From the point of view of this work, the two–term Debye model is especially important. It is not the best model for describing the complex permittivity of liquid samples (e.g., biomolecules of one type dissolved in pure water), but its main advantage is simplicity. The more variables the model has, the more problems it sets when fitting this model to real data. Therefore, the two–term Debye model will be used for the final fitting and interpolation of the obtained complex permittivity spectrum.
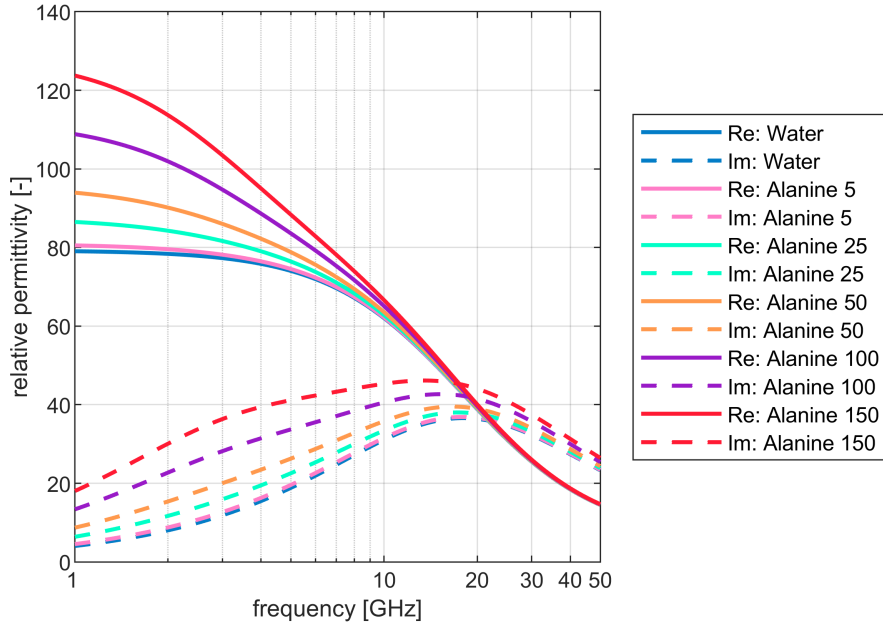
Figure 3.2: Two–term Debye model of complex water and alanine permittivity (1 - 50) GHz of various concentrations in mg/mL, based on eq. 3.16. The values of the parameters are [1, 2]: $\epsilon_h = 6.09$, $\epsilon_l = 79.27$, $\tau_1 = 8.84$ (ps), $\Delta = 1.63$, 8.17, 16.35, 32.70, 49.05, $\tau_2 = 0.50$ (ps) and from our measurement: $\sigma_l = 1$, 5.252, 6.004, 10, 14.21, 23.08 (µS/cm)

We can obtain the two–term Debye model by adding a second term in eq. (3.13), i.e.:

$$\epsilon^*(\omega) = \epsilon_h + \frac{\epsilon_l - \epsilon_h}{1 + i\omega\tau_1} + \frac{\Delta}{1 + i\omega\tau_2} + \frac{\sigma_l}{i\epsilon_0\omega}, \tag{3.16}$$

where τ_1 is the characteristic relaxation time of the first material (water), τ_2 is the characteristic relaxation time of the second material (dissolved biomolecules), and Δ is the dielectric increment of the second material. In the Figure 3.2, we can see the two–term Debye model for dissolved alanine in pure water of various concentrations.

For other models describing complex permittivity of water and amino acids see Section 3.3.2.

■ 3.3 Dielectric Properties of Materials

In this section, we will focus on the dielectric properties of materials relevant to this work.

■ 3.3.1 Water

Water is one of the basic building blocks of life, therefore it is essential to understand it. The water molecule is composed of an oxygen atom in the center and two light hydrogen atoms at two of its vertices. Its shape can be described as an almost regular tetrahedron [6].

The most important thing in our case is that the complex permittivity spectrum of water at low frequencies (assuming a constant temperature) can be well described by a Debye function [6].

■ 3.3.2 Amino Acids and Peptides

Amino acids are the basic building blocks of proteins and because of that a fundamental elements of life. So far, 20 biologically significant amino acids are known [6]. They can be classified into three groups:

- Hydrophilic – charged and polar

- Hydrophobic – nonpolar

- Special

In our case, the most important fact is the polar nature of amino acids in aqueous solutions. The dielectric properties of amino acids in aqueous solutions can thus be studied by broadband dielectric spectroscopy.

■ Dissolving Biomolecules in Water

Study of any polar molecule in aqueous solutions comprises the following two elementary tasks:

1. estimation of the molecule dipole moment (from literature, analytical models, etc.),

2. estimation of the relaxation time (from literature, analytical models, etc.).

Water and amino acids have both polar molecules, therefore at least two relaxation processes should occur in the permittivity spectrum [6]. The low frequency relaxation is credited to the rotation of the biomolecules, while the high frequency relaxation is assigned to the water dielectric properties. In its entirety, the entire dielectric spectrum of such a solution $\epsilon^*(\omega)$ can be described by the phenomenological Cole–Cole dispersion function [6]:

$$\epsilon^*(\omega) = \epsilon_h + \frac{\Delta\epsilon_1}{1 + (i\omega\tau_1)^{\alpha_1}} + \frac{\Delta\epsilon_2}{1 + (i\omega\tau_2)^{\alpha_2}}, \tag{3.17}$$

where ϵ_h is the high frequency limit of the permittivity, $\Delta\epsilon_1$ and $\Delta\epsilon_2$ are the corresponding relaxation strengths - dielectric increments, τ_1 and τ_2 are the relaxation times (Equation (3.9)) and α_1 and α_2 are shape parameters of the appropriate mode.

The amount of biomolecules dissolved in water has a direct effect on the complex permittivity of the water & biomolecules dielectric solution. The effect can be expressed by the dielectric increment $\Delta\epsilon$. We can write [4]:

$$\Delta\epsilon = \frac{N_V g p^2}{2k_B T \epsilon_0}, \tag{3.18}$$

where N_V is the density of the molecules, g is the correlation factor, p is the dipole moment of the molecules, T is the absolute temperature and k_B is the Boltzmann constant.

■ 3.4 Supplementary Section – Complex Dielectric Permittivity Sign Convention

For the following sections, it was necessary to determine the sign convention and adhere to it during the calculations. If we start from Maxwell's equations (Ampère's law), we can easily derive the sign convention:

$$\vec{\nabla} \times \vec{H} = \vec{J} + \frac{\partial \vec{D}}{\partial t}, \tag{3.19}$$

$$\vec{\nabla} \times \vec{H} = \sigma \cdot \vec{E} + \bar{\epsilon} \cdot \frac{\partial \vec{E}}{\partial t},$$

where

$$\vec{E} = \vec{E_0} \cdot e^{j\omega t}, \tag{3.20}$$

we can then write that:

$$\vec{\nabla} \times \vec{H} = \sigma \cdot \vec{E} + j\omega\bar{\epsilon} \cdot \vec{E},$$

$$\vec{\nabla} \times \vec{H} = j\omega\vec{E} \cdot \left(\underbrace{\bar{\epsilon} + \frac{\sigma}{j\omega}}_{\epsilon^*} \right), \qquad (3.21)$$

where ∇ is the nabla operator, $\vec{H}$ is the magnetic H field, $\vec{J}$ is the electric current density J field, $\vec{D}$ is the electric displacement D field, $\vec{E}$ is the intensity of the electric field, $\vec{E}_0$ is the constant intensity of the electric field, t is time, σ is conductivity, $\bar{\epsilon}$ is complex permittivity, j is the imaginary unit, ω is the angular frequency and ϵ^* is the total frequency-dependent complex permmittivity.

This sign convention (A) for ϵ^* will be followed during the work. See Table 3.1 for clarity on the possible transition between conventions:

A	B
$e^{j\omega t}$	$e^{-j\omega t}$
$\epsilon^* = \bar{\epsilon} - j\hat{\epsilon}$	$\epsilon^* = \bar{\epsilon} + j\hat{\epsilon}$
$\bar{\epsilon} + \dfrac{\sigma}{j\omega}$	$\bar{\epsilon} - \dfrac{\sigma}{j\omega}$

Table 3.1: Table of sign conventions.

where $\hat{\epsilon} = \dfrac{\sigma}{\omega}$.

Chapter 4

The Transmission Line

The transmission line for permittivity extraction is based on a conductor–backed coplanar waveguide (CBCPW) where the segment of the line dedicated to the sensing part is inverted. It consists of a middle ENIG (Electroless Nickel / Immersion Gold) copper conductor that is surrounded by a pair of ENIG copper ground conductors. The grounding conductors are then connected to the ground plate by vias (see Figure (4.1)). This transmission line was developed and tested in previous work [3].

Coplanar waveguide transmission lines are becoming a popular structure for low-volume permittivity measurements of liquid samples [13]. Their main advantages are:

1. confined fields in the slots

2. ease of fabrication

3. ease of integration into microfluidic structures
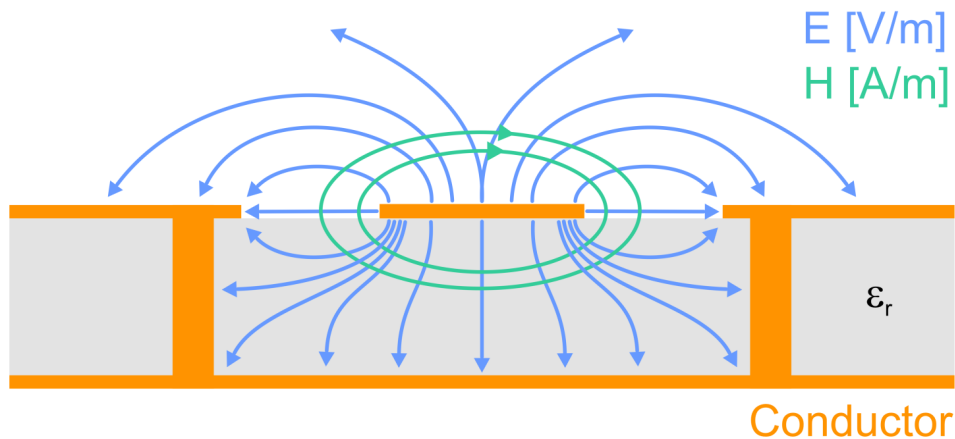
Figure 4.1: Side view of conductor–backed coplanar waveguide – ilustration by Ing. Daniel Havelka, Ph.D..

In our case, the measuring transmission line (see Figure (4.2)) is a modified CBCPW structure. The measuring area of the transmission line (delimited

15

by a green ellipse, see Figure (4.2)) is a 4 mm long CBCPW line, which is brought to the other side of the transmission line (ground plate side) by vias. The transmission line provides accurate reading regardless of the shape and volume of the material under test (for more info see [3]).
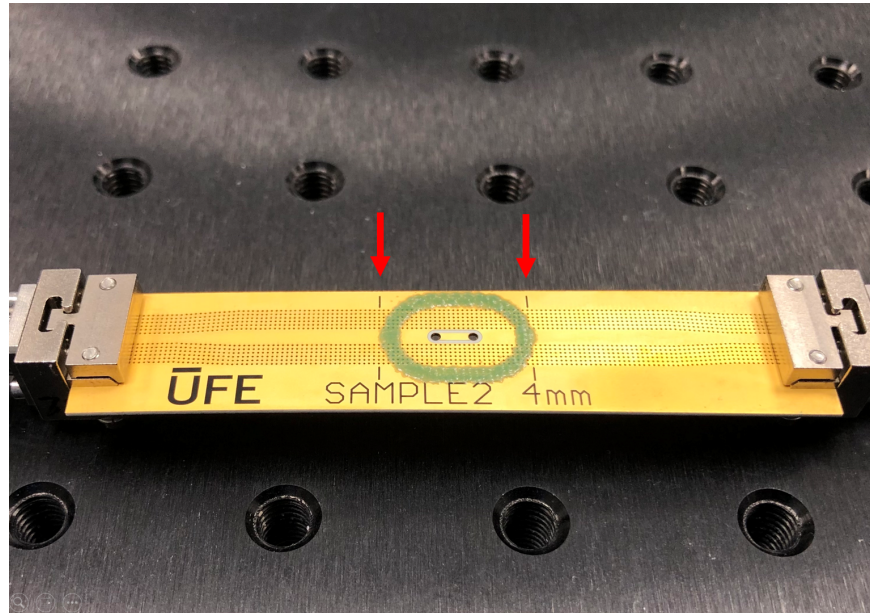
Figure 4.2: The measuring CBCPW transmission line, the black lines indicate the reference planes (red arrows).

Chapter 5

Theory of Permittivity Extraction from the Transmission Line

The basic idea of this method is to measure the propagation of electromagnetic signals (S–parameters) of a transmission line. When the sample is placed on the transmission line, the distribution of the electromagnetic field changes (see Chapter 4), and thus the S–parameters change. This change in the S–parameters allows us to calculate the complex permittivity of the material under test.

5.1   The Transmission Line Characterization

We start from the standard equation for the propagation constant γ and the characteristic impedance Z_0 of an arbitrary transmission line [24, eq. (37, 38), p. 541]:

$$\gamma = \sqrt{(j\omega L + R)(j\omega C + G)}, \tag{5.1}$$

$$Z_0 = \sqrt{(j\omega L + R)/(j\omega C + G)}, \tag{5.2}$$

where j is the imaginary unit, ω is angular frequency, L is inductance per length, R is resistance per length, C is capacitance per length and G is conductance per length (see [24, Fig. 1, p. 541].

Our transmission line will be calibrated with two liquid media, which means that we will get two propagation constants:

$$\gamma_1 = \sqrt{(j\omega L_1 + R_1)(j\omega C_1 + G_1)}, \tag{5.3}$$

$$\gamma_2 = \sqrt{(j\omega L_2 + R_2)(j\omega C_2 + G_2)}. \tag{5.4}$$

Due to the fact that the geometry and conductivity of the transmission line will be the same for both media and that the electromagnetic field interacts with biological samples mainly through the electrical component of the field (it therefore does not change the inductance of the transmission line), we can

say that [22]:

$$L_1 = L_2, \tag{5.5}$$

$$R_1 = R_2. \tag{5.6}$$

■ 5.1.1 Propagation Constant Extraction

From measurement and/or simulation, γ_1 can be obtained. γ_2 can be obtained from trace of measured wave–cascade matrices M_1, M_2 (also called chain transfer matrices, see [25, Fig. 2, eq. (6a, 6b)] for the definition):

$$M_1 = X \cdot R_1^{Z_0,Z_0}(l_1) \cdot Y, \tag{5.7}$$

$$M_2 = X \cdot R_2^{Z_0,Z_0}(l_2) \cdot Y, \tag{5.8}$$

where X,Y are matrices that represent the networks from the measurement planes to the transmission line and l_1, l_2 correspond to length of the transmission line segment loaded with the media. $R_1^{Z_0,Z_0}(l_1)$ and $R_2^{Z_0,Z_0}(l_2)$ represent the cascade matrices of the transmission lines referenced to a common reference impedance Z_0 at their input and output (see Figure 5.1).
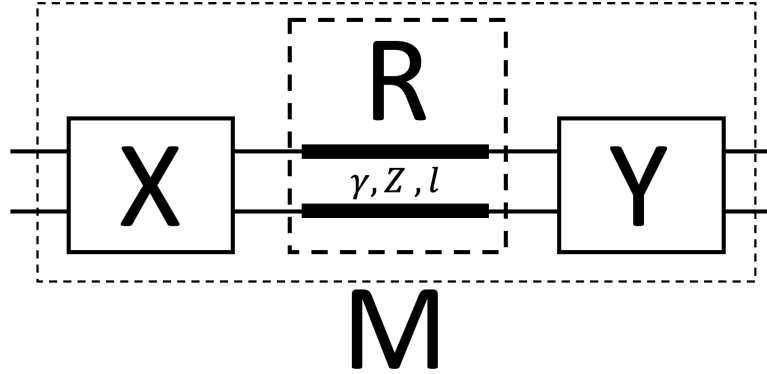
Figure 5.1: Composition of wave–cascade matrices M_1 and M_2.

For $R_1^{Z_0,Z_0}(l_1)$ holds:

$$R_1^{Z_0,Z_0}(l_1) = Q^{Z_0,Z_{c1}} \cdot R_1^{Z_{c1},Z_{c1}}(l_1) \cdot Q^{Z_{c1},Z_0}, \tag{5.9}$$

where $R_1^{Z_{c1},Z_{c1}}(l_1)$ represents the cascade matrix of the measuring surface of the transmission line with the first calibration medium referenced to the characteristic impedance Z_{c1} [24, eq. (38), p. 541], i.e.:

$$R_1^{Z_{c1},Z_{c1}}(l_1) = \begin{bmatrix} e^{-\gamma_1 \cdot l_1} & 0 \\ 0 & e^{\gamma_1 \cdot l_1} \end{bmatrix}. \tag{5.10}$$

The same relation as eq. (5.9) and (5.10) can be written as $R_2^{Z_0,Z_0}(l_2)$. The $Q^{Z_0,Z_{c1}}$ and Q^{Z_{c1},Z_0} are impedance transformers defined by [24, eq. (79), p. 548]:

$$Q^{Z_n, Z_m} = \frac{1}{2Z_m} \left| \frac{Z_m}{Z_n} \right| \sqrt{\frac{\Re(Z_n)}{\Re(Z_m)}} \begin{bmatrix} Z_m + Z_n & Z_m - Z_n \\ Z_m - Z_n & Z_m + Z_n \end{bmatrix}, \tag{5.11}$$

where Z_m, Z_n are the corresponding impedances and $\Re$ symbol refers to the real part of an imaginary number. The following relation can be derived from the Equations (5.7), (5.8) [22, eq. (10)]:

$$\operatorname{Tr}\left\{ M_2 \cdot M_1^{-1} \right\} =$$
$$2 \cdot \cosh\left(\gamma_1 \cdot l_1\right) \cosh\left(\gamma_2 \cdot l_2\right) - \left(\frac{Z_{c1}}{Z_{c2}} + \frac{Z_{c2}}{Z_{c1}}\right) \cdot \sinh\left(\gamma_1 \cdot l_1\right) \sinh\left(\gamma_2 \cdot l_2\right). \tag{5.12}$$

See annex (Section 10) for detailed derivation of eq. (5.12) from Equations (5.7), (5.8), (5.9), (5.10) and (5.11).

Since the length of the measuring surface of the transmission line will be the same for both calibration media, we can write that:

$$l_1 = l_2 = l. \tag{5.13}$$

Furthermore, since inductance L and resistance R in Z_{c1} and Z_{c2} will also be the same for both calibration media (L, R depend only on the conductor geometry and conductivity – see [22, eq. (11)]), based on eq. (5.5) and (5.6), we can write the following:

$$\frac{Z_{c1}}{Z_{c2}} = \sqrt{\frac{(j\omega L_{c1} + R_{c1})/(j\omega C_{c1} + G_{c1})}{(j\omega L_{c2} + R_{c2})/(j\omega C_{c2} + G_{c2})}} = \sqrt{\frac{(j\omega C_{c2} + G_{c2})}{(j\omega C_{c1} + G_{c1})}} = \frac{\gamma_2}{\gamma_1} \tag{5.14}$$

Based on Equations (5.13) and (5.14), we can rewrite Equation (5.12) in its final form:

$$\operatorname{Tr}\left\{ M_2 \cdot M_1^{-1} \right\} =$$
$$2 \cdot \cosh\left(\gamma_1 \cdot l\right) \cosh\left(\gamma_2 \cdot l\right) - \left(\frac{\gamma_1}{\gamma_2} + \frac{\gamma_2}{\gamma_1}\right) \cdot \sinh\left(\gamma_1 \cdot l\right) \sinh\left(\gamma_2 \cdot l\right). \tag{5.15}$$

From Equation (5.15) we can finally obtain γ_2 by numerical solver, because γ_2 is the only unknown. See Section 6 for more information.

5.1.2 Field Shape Factors Extraction

Thanks to the previous section, we have obtained numerical values for the propagation constants γ_1 and γ_2. To derive field shape factors, we start from Equation (5.3) for γ_1:

$$\gamma_1 = \sqrt{Z_{RL}} \cdot \sqrt{j\omega C_1 + G_1}, \tag{5.16}$$

where for simplicity:

$$Z_{RL} = j\omega L_1 + R_1. \tag{5.17}$$

The spatial area in which the measuring transmission line is located can be divided into two parts, above (surface area of the transmission line with the measured sample) and below (substrate) the transmission line (see Figure 5.2). We assume that all electromagnetic lines above the transmission line are contained within the sample.
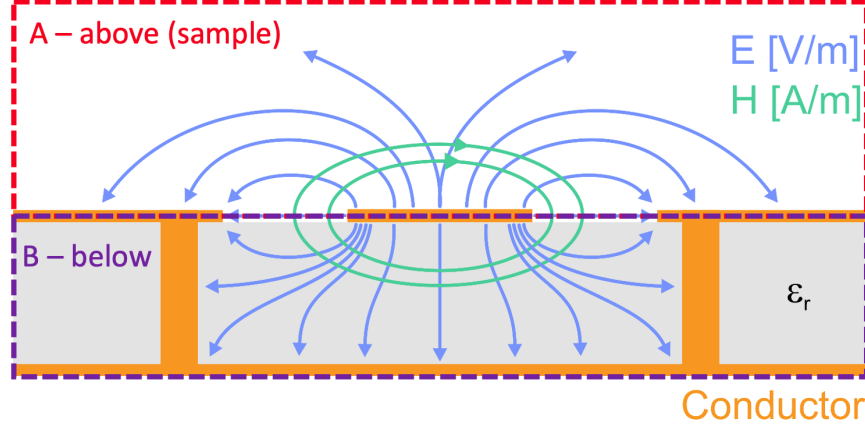
Figure 5.2: Spatial area of the transmission line divided into parts A and B.

Capacitance C and conductance G thus can be divided into a part A (above) and part B (below), i.e.:

$$C_1 = C_{1A} + C_{1B}, \tag{5.18}$$

$$G_1 = G_{1A} + G_{1B}. \tag{5.19}$$

Based on Equations (5.18) and (5.19), Equation (5.16) can be rewritten as:

$$\gamma_1 = \sqrt{Z_{RL}} \cdot \sqrt{j\omega(C_{1A} + C_{1B}) + G_{1A} + G_{1B}}, \tag{5.20}$$

The corresponding capacitances and conductances can be rewritten using the corresponding field shape factor K, the conductivity σ and the permittivity ϵ, i.e.:

$$C_{1A} = K_A \epsilon_{1A}, \tag{5.21}$$

$$C_{1B} = K_B \epsilon_{1B}, \tag{5.22}$$

$$G_{1A} = K_A \sigma_{1A}, \tag{5.23}$$

$$G_{1B} = K_B \sigma_{1B}. \tag{5.24}$$

After some equation manipulation and using Equations (5.21), (5.22), (5.23) and (5.24), Equation (5.20) can be rewritten as:

$$\gamma_1 = \sqrt{Z_{RL}} \cdot \sqrt{K_A(j\omega\epsilon_{1A} + \sigma_{1A}) + K_B(j\omega\epsilon_{1B} + \sigma_{1B})}, \tag{5.25}$$

In this way we get into the Equation (5.25) the field shape factors K_A and K_B that we are looking for. We now use the relation that the frequency-dependent complex permittivity ϵ^* is equal to (see Section 3.4):

$$\epsilon^* = \bar{\epsilon} + \frac{\sigma}{j\omega}, \tag{5.26}$$

where $\bar{\epsilon}$ is the complex permittivity, σ is the conductivity, and ω is the angular frequency. Using Equation (5.26), we obtain from Equation (5.25):

$$\gamma_1 = \sqrt{Z_{RL}} \cdot \sqrt{K_A j\omega\epsilon_{1A}^* + K_B j\omega\epsilon_{1B}^*}, \tag{5.27}$$

where ϵ_{1A}^* corresponds to the complex permittivity of the first calibration sample above the transmission line and ϵ_{1B}^* corresponds to the complex permittivity of substrate below the transmission line.

In the same way, we can derive for γ_2:

$$\gamma_2 = \sqrt{Z_{RL}} \cdot \sqrt{K_A j\omega\epsilon_{2A}^* + K_B j\omega\epsilon_{2B}^*}, \tag{5.28}$$

where ϵ_{2A}^* corresponds to the complex permittivity of the second calibration sample above the transmission line, ϵ_{2B}^* corresponds to the complex permittivity of the substrate below the transmission line and based on Equations (5.5) and (5.6) we assume [22, eq. (11)]:

$$j\omega L_1 + R_1 = j\omega L_2 + R_2 = Z_{RL}. \tag{5.29}$$

The electromagnetic field intensity above the transmission line will be affected by the enclosed measured sample, however, the field under the transmission line will always be the same. The transmission line substrate will not change between measurements. Based on that, we can write that:

$$\epsilon_{1B}^* = \epsilon_{2B}^* = \epsilon_S^*. \tag{5.30}$$

◼ 5.1.3 Solution of a System of Equations

From the previous section, we got a system of two complex equations with two unknowns K_A and K_B. Thus, on the basis of Equations (5.27), (5.28), (5.29) and (5.30):

$$\gamma_1 = \sqrt{Z_{RL}} \cdot \sqrt{K_A j\omega\epsilon_{1A}^* + K_B j\omega\epsilon_S^*}, \tag{5.31}$$

$$\gamma_2 = \sqrt{Z_{RL}} \cdot \sqrt{K_A j\omega\epsilon_{2A}^* + K_B j\omega\epsilon_S^*}. \tag{5.32}$$

From Equation (5.32) we express K_A:

$$\gamma_2^2 = Z_{RL} \cdot (K_A j\omega\epsilon_{2A}^* + K_B j\omega\epsilon_S^*)$$

$$\frac{\gamma_2^2}{Z_{RL}} - K_B j\omega\epsilon_S^* = K_A j\omega\epsilon_{2A}^*$$

$$K_A = \frac{1}{j\omega\epsilon_{2A}^*} \cdot \left(\frac{\gamma_2^2}{Z_{RL}} - K_B j\omega\epsilon_S^* \right). \tag{5.33}$$

Substituting Equation (5.33) into Equation (5.31) we get the following:

$$\gamma_1 = \sqrt{Z_{RL}} \cdot \sqrt{\frac{1}{j\omega\epsilon_{2A}^*} \cdot \left(\frac{\gamma_2^2}{Z_{RL}} - K_B j\omega\epsilon_S^* \right) \cdot j\omega\epsilon_{1A}^* + K_B j\omega\epsilon_S^*}$$

$$\frac{\gamma_1^2}{Z_{RL}} = \left(\frac{\gamma_2^2}{j\omega\epsilon_{2A}^* Z_{RL}} - \frac{K_B j\omega\epsilon_S^*}{j\omega\epsilon_{2A}^*}\right) \cdot j\omega\epsilon_{1A}^* + K_B j\omega\epsilon_S^*$$

$$\frac{\gamma_1^2}{Z_{RL}} = \frac{\gamma_2^2\epsilon_{1A}^*}{\epsilon_{2A}^* Z_{RL}} - \frac{K_B j\omega\epsilon_S^*\epsilon_{1A}^*}{\epsilon_{2A}^*} + K_B j\omega\epsilon_S^*$$

$$\frac{\gamma_1^2}{Z_{RL}} - \frac{\gamma_2^2\epsilon_{1A}^*}{\epsilon_{2A}^* Z_{RL}} = K_B \cdot \left(j\omega\epsilon_S^* - \frac{j\omega\epsilon_S^*\epsilon_{1A}^*}{\epsilon_{2A}^*}\right)$$

$$K_B = \frac{\dfrac{\gamma_1^2}{Z_{RL}} - \dfrac{\gamma_2^2\epsilon_{1A}^*}{Z_{RL}\epsilon_{2A}^*}}{j\omega\epsilon_S^* - \dfrac{j\omega\epsilon_S^*\epsilon_{1A}^*}{\epsilon_{2A}^*}}. \tag{5.34}$$

Substituting Equation (5.34) into Equation (5.33) we get K_A:

$$K_A = \frac{1}{j\omega\epsilon_{2A}^*} \cdot \left(\frac{\gamma_2^2}{Z_{RL}} - \frac{\dfrac{\gamma_1^2}{Z_{RL}} - \dfrac{\gamma_2^2\epsilon_{1A}^*}{Z_{RL}\epsilon_{2A}^*}}{j\omega\epsilon_S^* - \dfrac{j\omega\epsilon_S^*\epsilon_{1A}^*}{\epsilon_{2A}^*}} \cdot j\omega\epsilon_S^*\right)$$

$$K_A = \frac{1}{j\omega\epsilon_{2A}^*} \cdot \left(\frac{\gamma_2^2}{Z_{RL}} - \left[\frac{\gamma_1^2}{Z_{RL}} - \frac{\gamma_2^2\epsilon_{1A}^*}{Z_{RL}\epsilon_{2A}^*}\right] \cdot \left[\frac{\epsilon_{2A}^*}{j\omega\epsilon_S^*\epsilon_{2A}^* - j\omega\epsilon_S^*\epsilon_{1A}^*}\right] \cdot j\omega\epsilon_S^*\right)$$

$$K_A = \frac{1}{j\omega\epsilon_{2A}^*} \cdot \left(\frac{\gamma_2^2}{Z_{RL}} - \left[\frac{\gamma_1^2}{Z_{RL}} - \frac{\gamma_2^2\epsilon_{1A}^*}{Z_{RL}\epsilon_{2A}^*}\right] \cdot \left[\frac{\epsilon_{2A}^*}{\epsilon_{2A}^* - \epsilon_{1A}^*}\right]\right). \tag{5.35}$$

In addition, based on Equations (5.1), (5.2) and (5.29) we can use a trick for the numerical value of Z_{RL}, that is:

$$Z_{RL} = \gamma_1 \cdot Z_1 =$$

$$\sqrt{(j\omega L_1 + R_1)(j\omega C_1 + G_1)} \cdot \sqrt{\frac{(j\omega L_1 + R_1)}{(j\omega C_1 + G_1)}} = j\omega L_1 + R_1. \tag{5.36}$$

Finally, by simplifying Equations (5.35) and (5.34) we obtain the final form of K_A and K_B, that is:

$$K_A = \frac{\gamma_1^2 - \gamma_2^2}{j\omega Z_{RL}(\epsilon_{1A}^* - \epsilon_{2A}^*)} \tag{5.37}$$

$$K_B = \frac{\gamma_2^2\epsilon_{1A}^* - \gamma_1^2\epsilon_{2A}^*}{j\omega Z_{RL}\epsilon_S^*(\epsilon_{1A}^* - \epsilon_{2A}^*)} \tag{5.38}$$

■ **5.2   Permittivity of the Material under Test**

Thanks to the previous sections, we have a characterized transmission line in the form of the propagation constant γ_1 and the field shape factors K_A and K_B. We will now obtain a procedure for obtaining complex permittivity from this data.

We start with the Equation (5.15):

$$\text{Tr}\left\{M_3 \cdot M_1^{-1}\right\} =$$
$$2 \cdot \cosh(\gamma_1 \cdot l)\cosh(\gamma_3 \cdot l) - \left(\frac{\gamma_1}{\gamma_3} + \frac{\gamma_3}{\gamma_1}\right) \cdot \sinh(\gamma_1 \cdot l)\sinh(\gamma_3 \cdot l), \quad (5.39)$$

where M_3, M_1 (wave-cascade matrices) are obtained from the measured data (see Section 5.1.1), γ_1 is the propagation constant of the first calibration medium, l is the measurement surface length of the transmission line, and γ_3 is the propagation constant of the material under test (MUT). The γ_3 is the only unknown and we obtain it by numerical solution of eq. 5.39.

Subsequently, we divide γ_1 by γ_3 and based on the Equation (5.27), we obtain:

$$\frac{\gamma_1}{\gamma_3} = \sqrt{\frac{K_B j\omega\epsilon_s^* + K_A j\omega\epsilon_{1A}^*}{K_B j\omega\epsilon_s^* + K_A j\omega\epsilon_{3A}^*}}, \quad (5.40)$$

where ϵ_s^* is the complex permittivity of the substrate, ϵ_1^* is the complex permittivity of the first calibration medium and ϵ_3^* is the unknown complex permittivity. By expressing ϵ_3^* from the Equation (5.40), we then obtain the required permittivity of the MUT, i.e.:

$$\left(\frac{\gamma_1}{\gamma_3}\right)^2 = \frac{K_B j\omega\epsilon_s^* + K_A j\omega\epsilon_{1A}^*}{K_B j\omega\epsilon_s^* + K_A j\omega\epsilon_{3A}^*}$$

$$K_B j\omega\epsilon_s^* + K_A j\omega\epsilon_{3A}^* = \left[K_B j\omega\epsilon_s^* + K_A j\omega\epsilon_{1A}^*\right] \cdot \left(\frac{\gamma_3}{\gamma_1}\right)^2$$

$$\epsilon_{3A}^* = \frac{\left[K_B\epsilon_s^* + K_A\epsilon_{1A}^*\right] \cdot \left(\dfrac{\gamma_3}{\gamma_1}\right)^2 - K_B\epsilon_s^*}{K_A} \quad (5.41)$$

This is possible because in Equation (5.40), ϵ_3^* is the only unknown.

Chapter 6

Implementation of Permittivity Extraction from the Transmission Line

The aim of this chapter is to provide a detailed description of the implementation of the method. The whole method is implemented in MATLAB. For ease of understanding, Figure 6.1 shows a simplified diagram of the method. The goal of this schema is to capture the flow of data through the method.
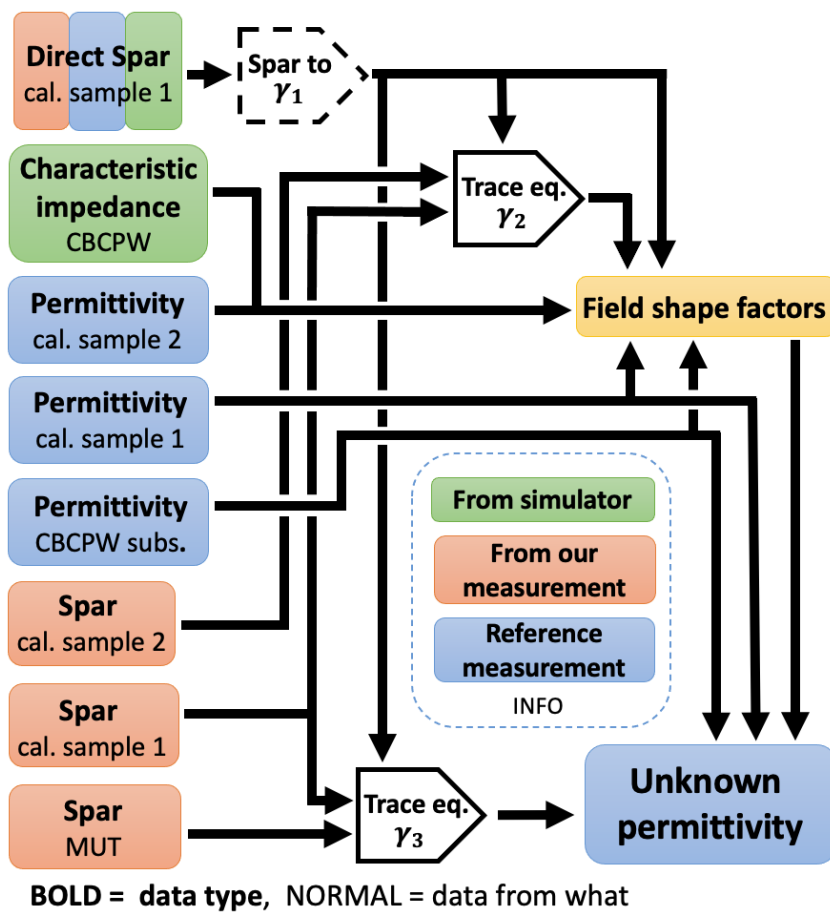
Figure 6.1: Simplified scheme of the complex permittivity extraction method.

The method can be divided into two basic parts:

1. Coplanar transmission line characterization

2. Complex permittivity extraction

Coplanar transmission line characterization is performed once. Subsequently, we insert the measured S parameters of the MUT (material under test) into the method. The result is the required complex permittivity of the MUT.

The division of sections in this chapter corresponds to the course of the method. At the beginning of each section are its inputs and outputs. It is important to note that the procedure described in this chapter is performed many times - once for each measured frequency point.

6.1 Transmission Line Characterization

6.1.1 S–parameters Transformation

Input:

- S–parameters – magnitude and phase format

Output:

- S–parameters – complex number format

S–parameters are often in magnitude and phase format. Before entering the method, it is necessary to convert them to S–parameters in complex number format, i.e.:

$$x = 10^{(Mag/20)} \cdot [\cos(Pha) + i \cdot \sin(Pha)], \qquad (6.1)$$

where Mag is the magnitude of the input S–parameters, Pha is the phase of the input S–parameters and x are the S–parameters in the complex number format.

6.1.2 Data Interpolation

Input:

- Any data

Output:

- Any data

The measured data and the data from the simulator/reference measurement often do not have the same length – they are not from the same frequency points. Before using the method, all data must be interpolated to the same frequency points. In our case, the data from the reference measurement were interpolated to the frequency points of the real measured data from the vector network analyzer.

Spline smoothing interpolation can be used for interpolation.

6.1.3 First Calibration Sample Propagation Constant from ABCD Matrix

Input:

- S–parameters from the simulator

Output:

- Propagation constant γ_1 of the CBCPW line with the first calibration medium

First we need to obtain the value of a propagation constant of the first calibration medium. One option would be to obtain the propagation constant from measurement. This might be rather easy for an empty transmission line (i.e. loaded by air only, which does not represent a good calibration medium, since its permittivity is far from water-based biological media), but is much more complicated for liquid samples. To that end, it would be necessary to eliminate all other sections of the CBCPW line (with air, etc.), transitions and so on, by de-embedding.

For these reasons, decided we obtain γ_1 from the simulator (based on our and reference measurement). In the simulator, we define a short section of the CBCPW line with only the first calibration medium. We then obtain the S–parameters of the line section with reference planes directly on the first calibration medium. The S–parameters than can be converted to the propagation constant γ_1. We can use ABCD parameters to convert S–parameters to the propagation constant. We first convert the S–parameters to the ABCD parameters [25]:

$$A = \frac{(1 + S_{11}) \cdot (1 - S_{22}) + S_{12}S_{21}}{2S_{21}}, \tag{6.2}$$

$$D = \frac{(1 - S_{11}) \cdot (1 + S_{22}) + S_{12}S_{21}}{2S_{21}}, \tag{6.3}$$

where A and D are parts of the ABCD matrix, and S_{11}, ..., S_{22} are the S–parameters from simulator. Substituting Equations (6.2) and (6.3) into Equation (6.4), we obtain the propagation constant of the first calibration medium γ_1 [26], that is:

$$\gamma_1 = \frac{\text{arcCosh}(\sqrt{A \cdot D})}{l}, \tag{6.4}$$

where l is the length of the section of the CBCPW line.

6.1.4 Second Calibration Sample Propagation Constant

Input:

- Measured S–parameters of the first calibration sample

27

- Measured S–parameters of the second calibration sample

- Propagation constant γ_1 of the CBCPW line of the first calibration sample

Output:

- Propagation constant γ_2 of the CBCPW line of the second calibration sample

This section is based on Section 5.1.1, specifically Equation (5.15). Propagation constant γ_2 of the second calibration sample can be obtained using numerical solver. Because Equation (5.15) is complex, γ_2 can have multiple solutions. It is therefore important to set the numeric solver in such a way that it behaves deterministically and converges to the same solutions under the same initial conditions.

▪ 6.1.5 Field Shape Factors Extraction

Input:

- Propagation constant γ_1 of the first calibration sample

- Propagation constant γ_2 of the second calibration sample

- Permittivity ϵ_{1A}^* of the first calibration sample

- Permittivity ϵ_{2A}^* of the second calibration sample

- Permittivity ϵ_S^* of the CBCPW line substrate

- Characteristic impedance Z_1 of the CBCPW line.

Output:

- Field shape factors K_A and K_B.

This section is based on Section 5.1.3, specifically Equations (5.37) and (5.38). Obtained field shape factors K_A and K_B are the main result of the transmission line characterization phase.

▪ 6.2 Complex Permittivity Extraction

The procedure in this section will be shown specifically on MUT alanine 100 mg/mL, calibration solutions water and water with alanine 50 mg/mL. However, the procedure can be generalized to any sample with a permittivity close to that of the calibration solutions.

6.2.1 Areas of Validity of the Solution

Input:

- Measured S–parameters of the first calibration sample

- Measured S–parameters of the second calibration sample

- Propagation constant γ_1 of the CBCPW line of the first calibration sample

- Propagation constant γ_2 of the CBCPW line of the second calibration sample

Output:

- Areas of validity of the solution for Section 6.2.3

In this section, we try to find permittivity of the MUT. We try to achieve this using the field shape factors, which were calculated from the propagation constant of the second calibration sample. Ideally, Equation (5.15), from Section 5.1.1, would apply in all cases. In practice, however, this is not the case, because the equation contains complex hyperbolic functions.

Complex hyperbolic functions consist of exponentials, which means that they can quickly reach very large values. Ideally, there would be no problem with absolute numerical accuracy. In practice, however, the numbers are stored on a computer with limited numerical accuracy – each value is rounded. Thanks to complex hyperbolic functions, these small inaccuracies can multiply into huge values.

In practice, therefore, we must substitute the input values into the Equation (5.15) and check whether the equation holds. If the error of the equation exceeds a certain limit, its results for the given frequency points cannot be used for further calculations.

In Section 6.2.3 in Figures 6.6 and 6.7 we can see in the range 20 – 25 GHz that the permittivity results do not correspond well. This area corresponds to the area where Equation (5.15) does not give the correct solutions. Therefore, results in this frequency range cannot be used.

6.2.2 Third Propagation Constant of the MUT

Input:

- Measured S–parameters of the first calibration sample

- Measured S–parameters of the MUT

- Propagation constant γ_1 of the CBCPW line of the first calibration sample

Output:

- Propagation constants γ_3 of the CBCPW line of the MUT

This section is based on Section 5.2, specifically Equation (5.39). The beauty of Equation (5.39) is that it allows us to determine propagation constant from S–parameters without direct measurement, which is very difficult. However, the problem is the complexity of this equation.

Equation (5.39) does not give an unambiguous solution. If we convert the Equation (5.39) into the following form:

$$0 = 2 \cdot \cosh\left(\gamma_1 \cdot l\right)\cosh\left(\gamma_3 \cdot l\right) - \left(\frac{\gamma_1}{\gamma_3} + \frac{\gamma_3}{\gamma_1}\right) \cdot \sinh\left(\gamma_1 \cdot l\right)\sinh\left(\gamma_3 \cdot l\right)$$
$$- \operatorname{Tr}\left\{M_3 \cdot M_1^{-1}\right\}, \quad (6.5)$$

insert any actual values obtained by the previous steps:

$$l = 0.004 \; [\mathrm{m}]$$
$$\gamma_1 = 0.12 + 34.14i \; [1/\mathrm{m}]$$
$$\operatorname{Tr}\left\{M_3 \cdot M_1^{-1}\right\} = 1.99 + 1.50i$$

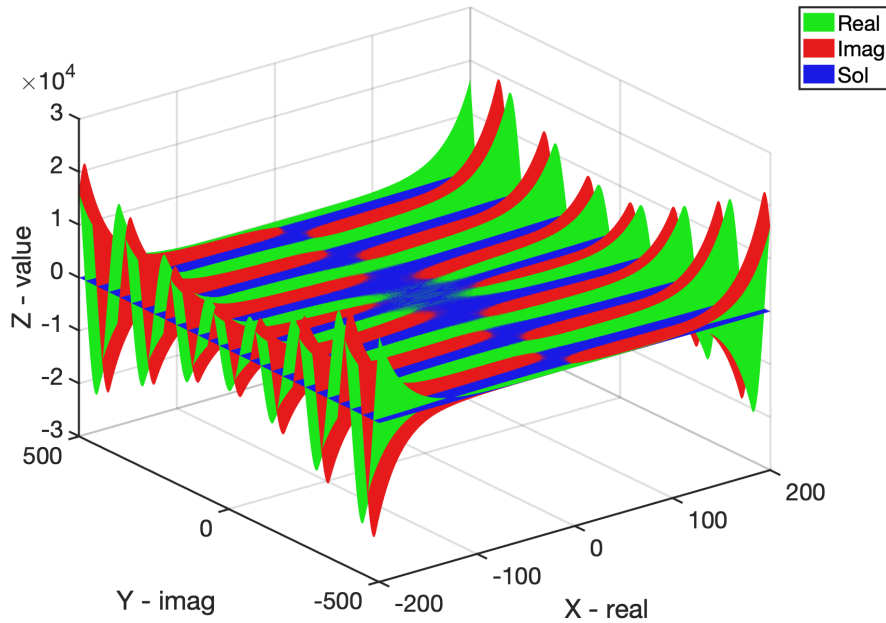and plot the output for unknown γ_3, we get Figure 6.2.

Figure 6.2: Complex Equation (6.5) for unknown γ_3.

In Figure 6.2 we have a complex plane plotted on the x and y axes. The z-axis corresponds to the output value of the complex function. The green area corresponds to the real component of the function. The red area corresponds to the imaginary component of the function. The blue area is then the complex plane itself corresponding to the x and y axes. Where the red and blue areas simultaneously intersect the blue area, there is a solution to Equation (6.5). If we draw only the solutions map in 2D space (areas where the red and

green areas simultaneously approach zero), we get Figure 6.3. The yellow area corresponds to the solution of Equation (6.5) whenever the real and imaginary output components were simultaneously less than 2. However, if we increase the resolution and look at the solution map in more detail, we will find that each yellow area contains whole nests of other solutions.

The solution of Equation (6.5) cannot be expressed analytically. The equation can be solved using a numeric solver, but it is obvious that the solver converges to different solutions based on the different initial conditions. Each of the solutions then results in a different complex permittivity of the MUT.

The solution to this problem is to run the numeric solver many times with random initial conditions. The goal is to obtain as many independent γ_3 solutions as possible, which will be further processed.
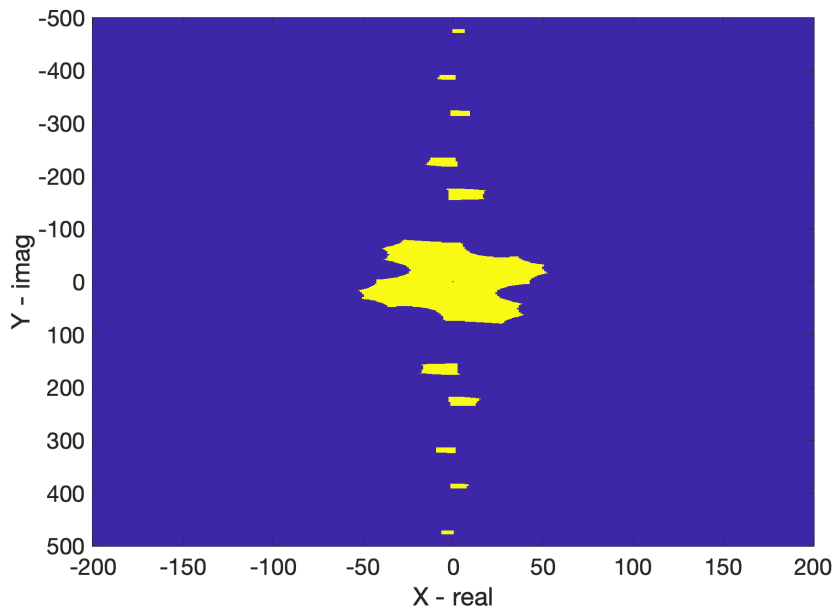

Figure 6.3: 2D map of solutions of Equation (6.5), yellow color corresponds to solution.

■ 6.2.3 Choice of the Right Propagation Constant of the MUT

Input:

- Propagation constants γ_3 of the CBCPW line of the MUT

Output:

- Selected solutions of the propagation constants γ_3 of the CBCPW line of the MUT

Consider, for example, calibration solutions of water and water with alanine 50 mg/mL. Our MUT will be water with alanine 100 mg/mL. If we sort the

calculated γ_3 from the previous section based on its size (absolute values of the complex number), we get Figure 6.4 and Figure 6.5.

If we then calculate the corresponding permittivity for these sorted γ_3 on the basis of Section 5.2, we obtain Figures 6.6 and 6.7. As we can see, the solutions with the smallest absolute value achieve the best values of the resulting permittivity. These are the base solutions, where higher harmonic solutions no longer achieve such good results. We will select the first two absolutely smallest γ_3 as the solution of Equation (6.5) (Figure 6.5, Abs 1 and Abs 2).

Although this example of a selection of the propagation constant of the MUT was shown for alanine 100 mg/mL only, this procedure can be generalized to any other liquid samples close to the calibration media.
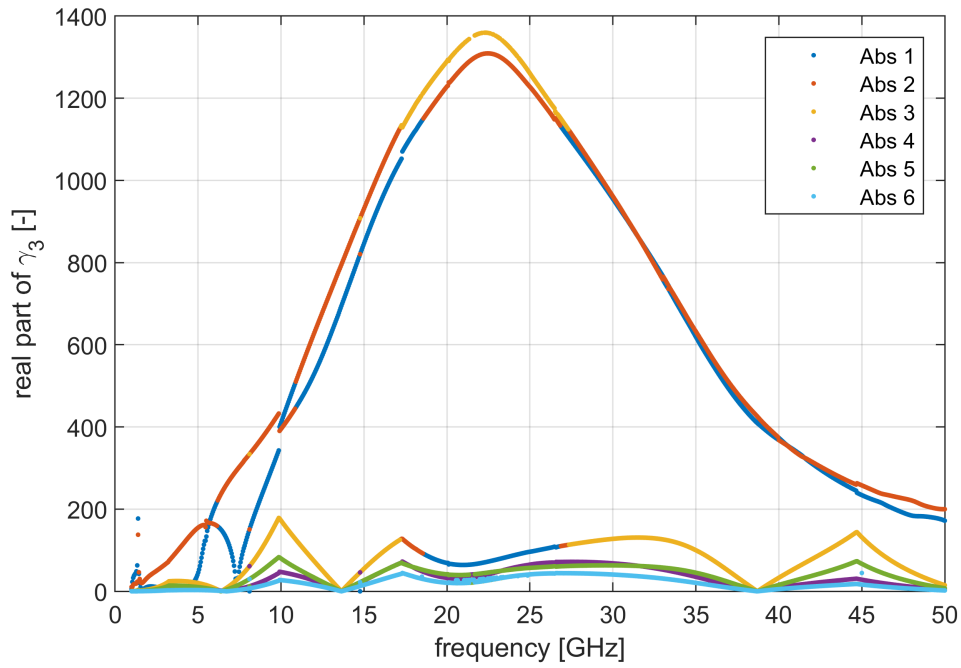
Figure 6.4: Real part of values of the sorted γ_3 by their absolute value, Abs 1 corresponds to the smallest solution.
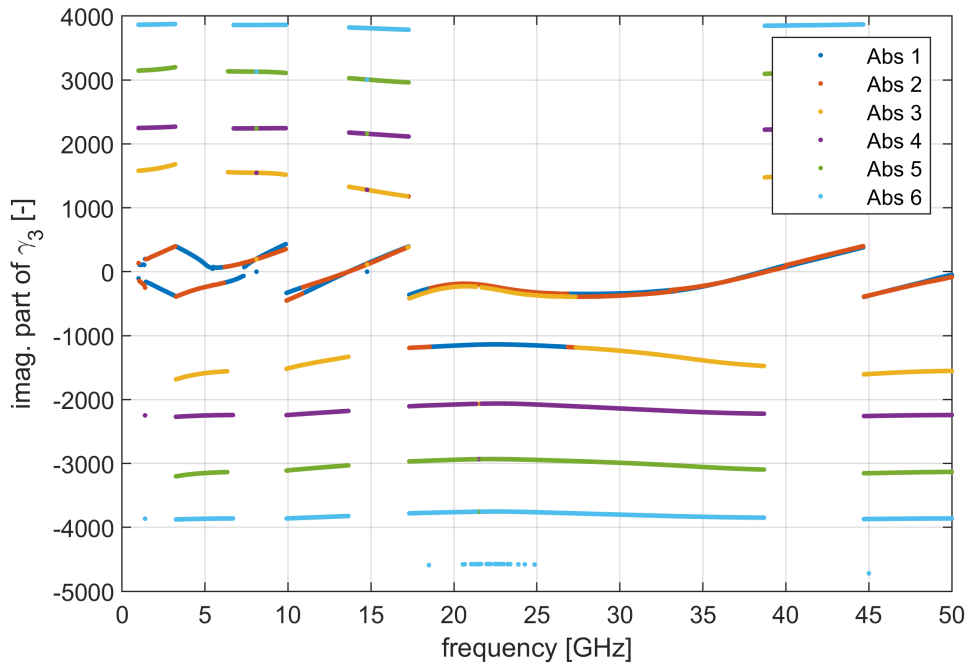

Figure 6.5: Imaginary part of values of the sorted γ_3 by their absolute value, Abs 1 corresponds to the smallest solution.

33

Figure 6.6: Real values of permittivity of the MUT based on the sorted γ_3, Abs 1 corresponds to the smallest solution, REF is the reference permittivity.

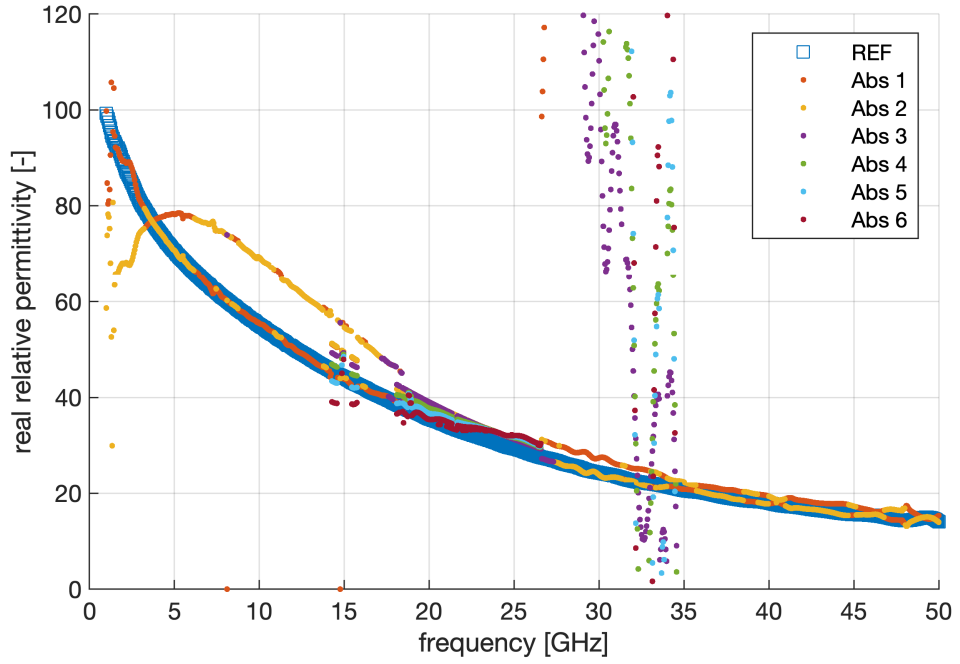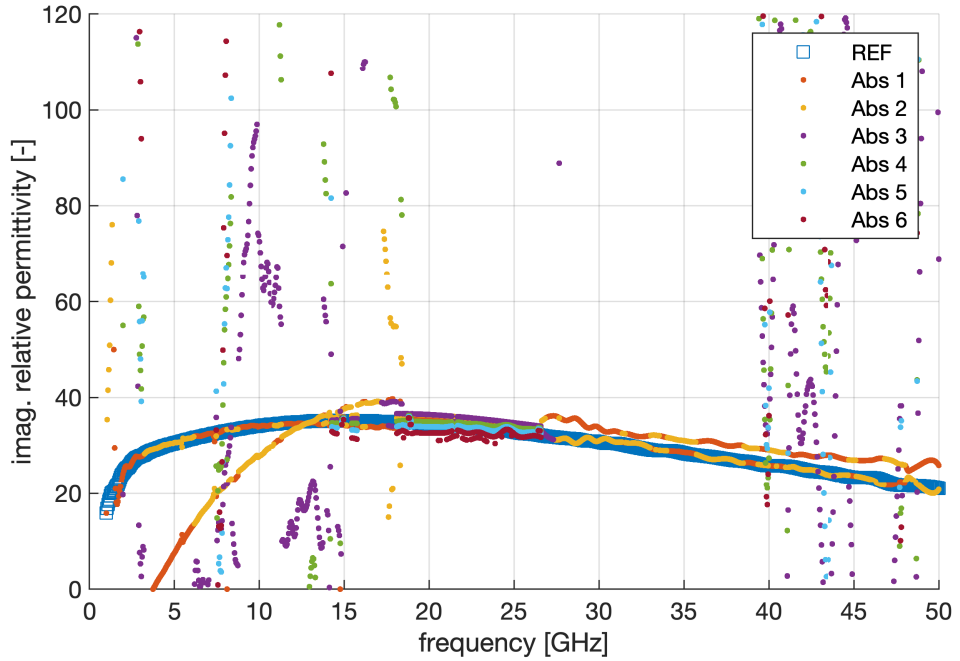**Figure 6.7:** Imaginary values of permittivity of the MUT based on the sorted γ_3, Abs 1 corresponds to the smallest solution, REF is the reference permittivity.

▇ 6.2.4 Permittivity Extraction

Input:

- Selected solutions of the propagation constants γ_3 of the CBCPW line of the MUT

Output:

- Permittivity of the MUT at certain frequency points

Using the procedure described in the previous section, we have selected γ_3 propagation constants, from which we calculate the unknown permittivity of the MUT (based on Section 5.2). The output can be seen in Figures 6.6 and 6.7 (red and yellow curves corresponding to Abs 1 and Abs 2).

In Figure 6.8 we can see the imaginary component of the solutions of Abs 1 and Abs 2. As we can see, these are the base solutions for the γ_3 that are very close in value, but have a different final permittivity of the MUT. The numerical solver jumps between these two solutions, as is evident in Figure 6.8. At the same time, we can see that the Abs 1 and Abs 2 solutions behave like their complements, mirroring each other.
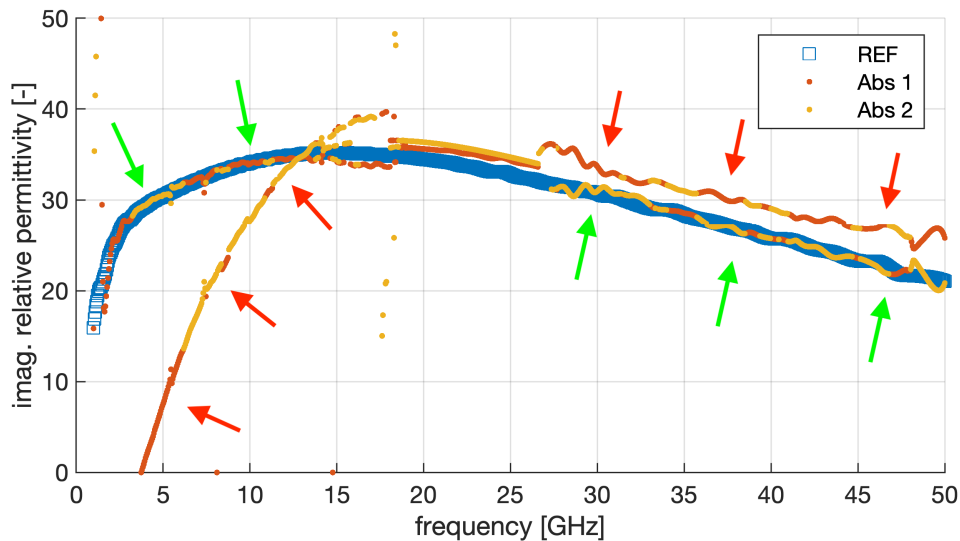

Figure 6.8: Imaginary values of permittivity of the MUT based on the sorted γ_3 – Abs 1 and Abs 2.

In Figure 6.8 we can see two main courses of the solution. The correct solution is marked with green arrows, and the wrong solution is marked with red arrows. Our goal is to separate the two solutions. From Section 6.2.1 we know that the intervals for correct solutions are approximately 0 to 12 GHz and 28 to 50 GHz. We just need to interpolate the permittivity solution for Abs 1 and Abs 2 with a suitable curve that separates the upper and lower course of the solution. In the interval 0 to 12 GHz, we will consider only

the upper part of the solutions (above the separating curve), in interval 28 to 50 GHz we will consider only the lower part of the solutions (below the separating curve).

In Figure 6.9 we can see a specific example for the permittivity solution corresponding to Abs 1 (γ_3). The separating function here is a fourth degree polynomial function. The solution areas are indicated by green arrows.

Figure 6.9: Solution of permittivity corresponding to Abs 1 separated by polynomial of fourth degree.

Following the same procedure as in Figure 6.9, we obtain a solution for permittivity corresponding to Abs 2 (γ_3). Although we did separation for the imaginary parts of the solutions, we also separated the real parts of the solutions. We then add the resulting permittivity solutions for Abs 1 and Abs 2 into one result.

■ 6.2.5 Interpolation of the Resulting Permittivity by the Debye Model

Input:

- Permittivity of the MUT at certain frequency points

Output:

- Interpolated Permittivity of the MUT for the whole frequency spectrum

We now have the resulting MUT permittivity data. However, the data is fragmentary, not continuous across the spectrum, wavy, and contains outliers caused by numerical errors. Therefore, it would be good to interpolate the data with a suitable curve, capturing the physical nature of the thing.

We will use the two–term Debye model (Section 3.2.2) for the final fit of the data in the following way.

36

1. Use an optimizer to fit the data using the Debye two–term model.

2. Find in the data the farthest point from the two–term Debye model and remove it.

3. Return to point 1. until the distance of the furthest point from the model reaches a certain threshold value.

This self–tuning procedure removes outliers and gives us the desired smoothed complex permittivity over the entire measured frequency spectrum.

Chapter 7

Final Measurement

Here we describe materials and methods used to obtain the experimental data for this thesis. The amino-acid samples were prepared from L-alanine (purity 98.5 % , P-Lab CZ, R30761) and L-cysteine (purity 98% , P-Lab, C 10502) powder for the sample preparation. The powder was dissolved in milipore-Q water to obtain the requested concentrations. The course of the final measurement of S–parameters can be seen in Figure 7.1. The S–parameters were measured using vector network analyzer Rohde & Schwarz – ZVA 67, from 1.5 to 50 GHz at 1601 frequency points. The assembly was first calibrated with a custom calibration set, consisting of sections of CBCPW lines of different lengths (1,2,4,8 mm), thru, short (see Figure (7.2)). Subsequently, the measurement itself began.
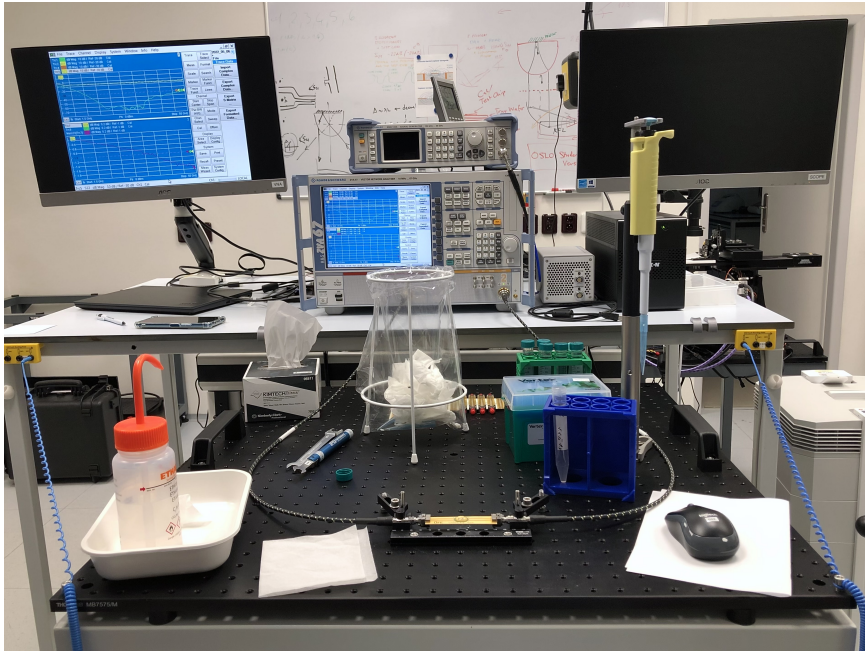
Figure 7.1: The experimental setup of the final measurement.

Each sample was measured five times. Between samples, the transmission line was cleaned with isopropyl alcohol and dried with nitrogen. In Figure 7.3,

we can see the transmission line with a liquid sample. Throughout the measurement, the temperature was maintained at 23°C and the relative humidity at 45 %.
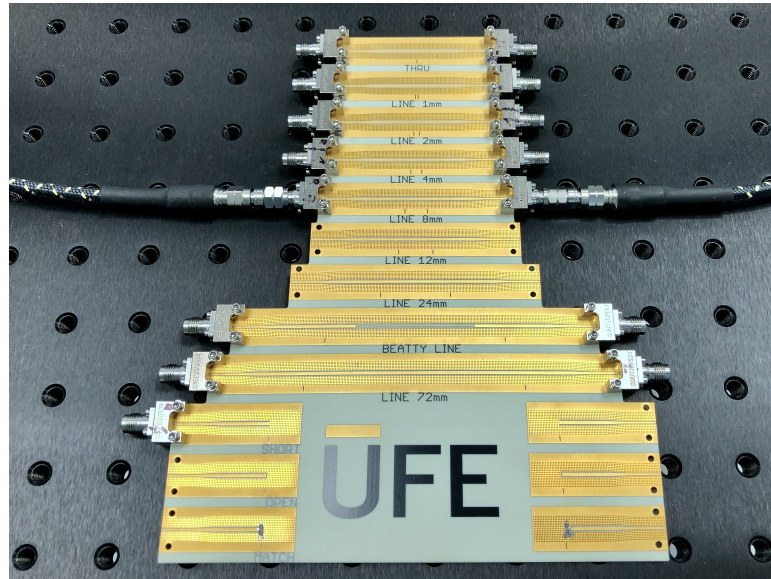

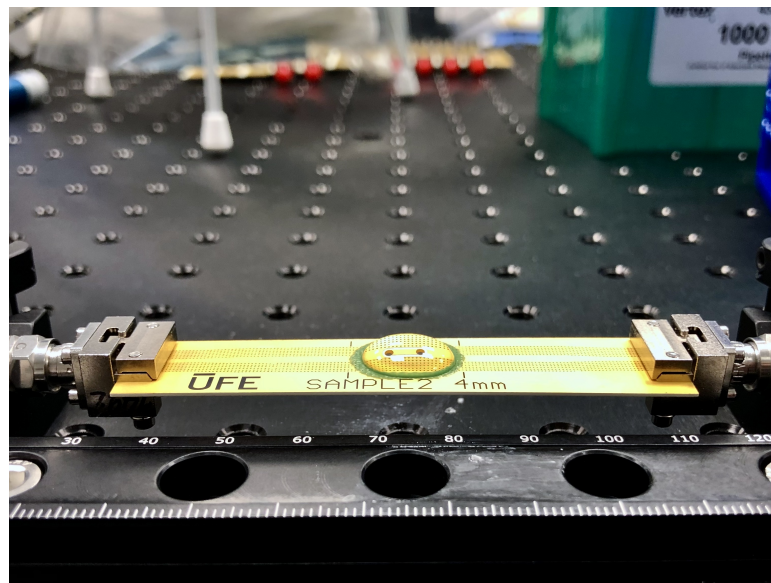**Figure 7.2:** Multiline TRL calibration kit for the CBCPW transmission line.

Figure 7.3: The CBCPW transmission line with a liquid sample (250 μL).

Chapter 8

The Resulting Acquired Pemitivity

8.1 Simulator/Reference Measurement

The method was first tested on ideal data from the simulator/reference measurement, CST microwave studio. Water and water with alanine 50 mg/mL were used as the calibration solutions. We can see the results in Figures 8.1 and 8.2.
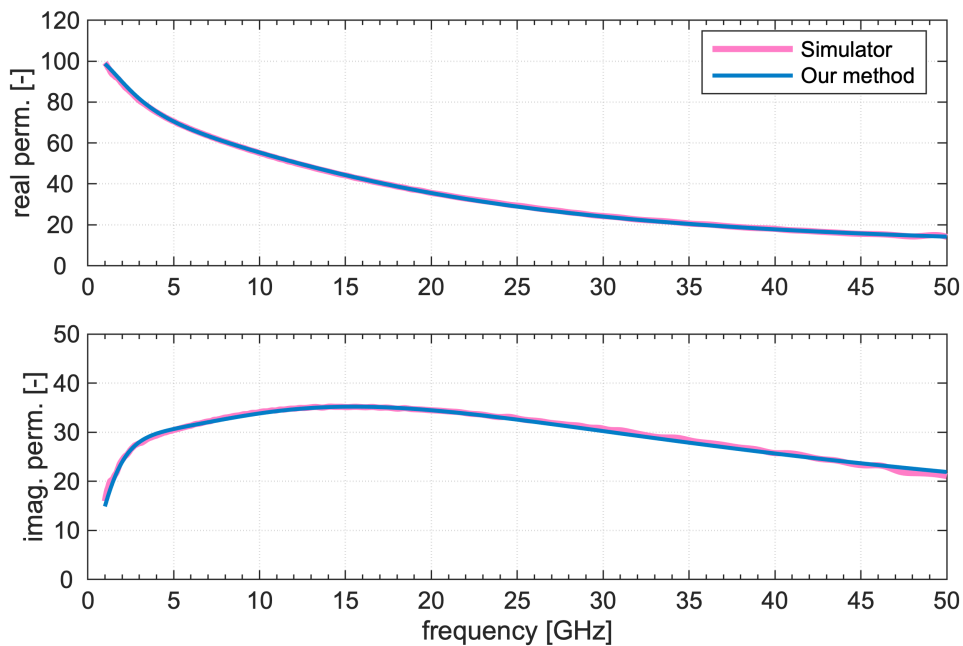
8.1.1 Alanine 100 mg/mL

Figure 8.1: Complex permittivity from simulator/reference measurement and from our method – **MUT alanine 100 mg/mL**.
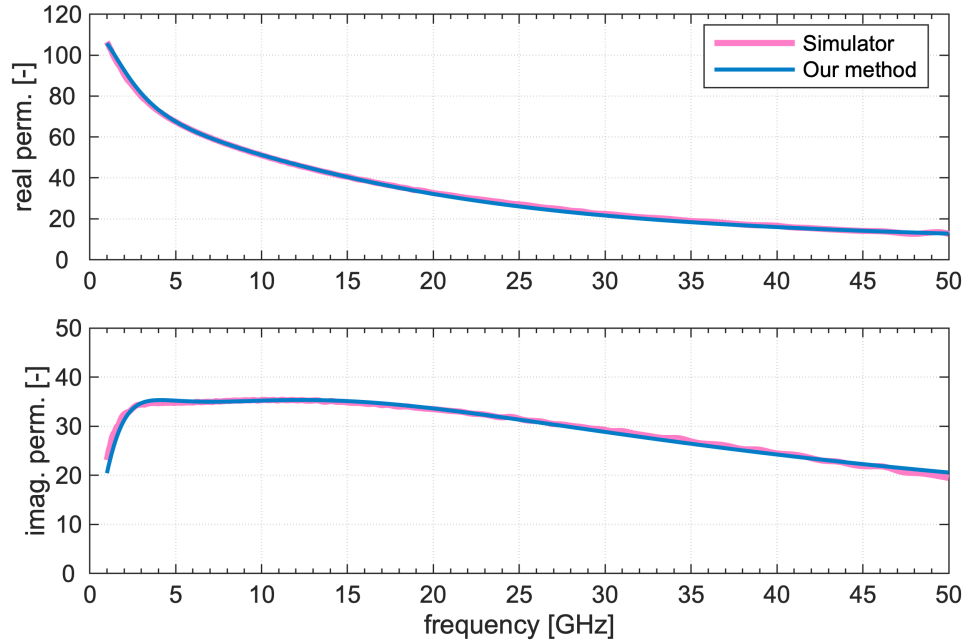
8.1.2   Alanine 150 mg/mL

Figure 8.2: Complex permittivity from simulator/reference measurement and from our method – **MUT alanine 150 mg/mL**.

8.2   Real Measured Data

In this section, we describe the main results of this work. The measured water and water with alanine 50 mg/mL samples were used as the calibration solutions. The other necessary inputs were obtained from the simulator/reference measurement (for more information, see Section 6).

Figures 8.3, 8.5, 8.7, 8.9, and 8.11 show the results of the complex permittivity obtained by our method compared to the results measured by another independent method, which employs an open-ended coaxial probe [3]. The orange line is the absolute difference in permittivity between those two methods. Each sample was measured five times. The previous figures, therefore, show the average of the five repetitions of the extracted complex permittivity. In Figures 8.4, 8.6, 8.8, 8.10 and 8.12 we can then see the standard deviation calculated from these five measurements for each sample.

It is important to say that the samples we measured were different from the samples measured by the reference method, although the concentrations were the same. Furthermore, the samples that we measured had a different temperature than those measured by the reference method.
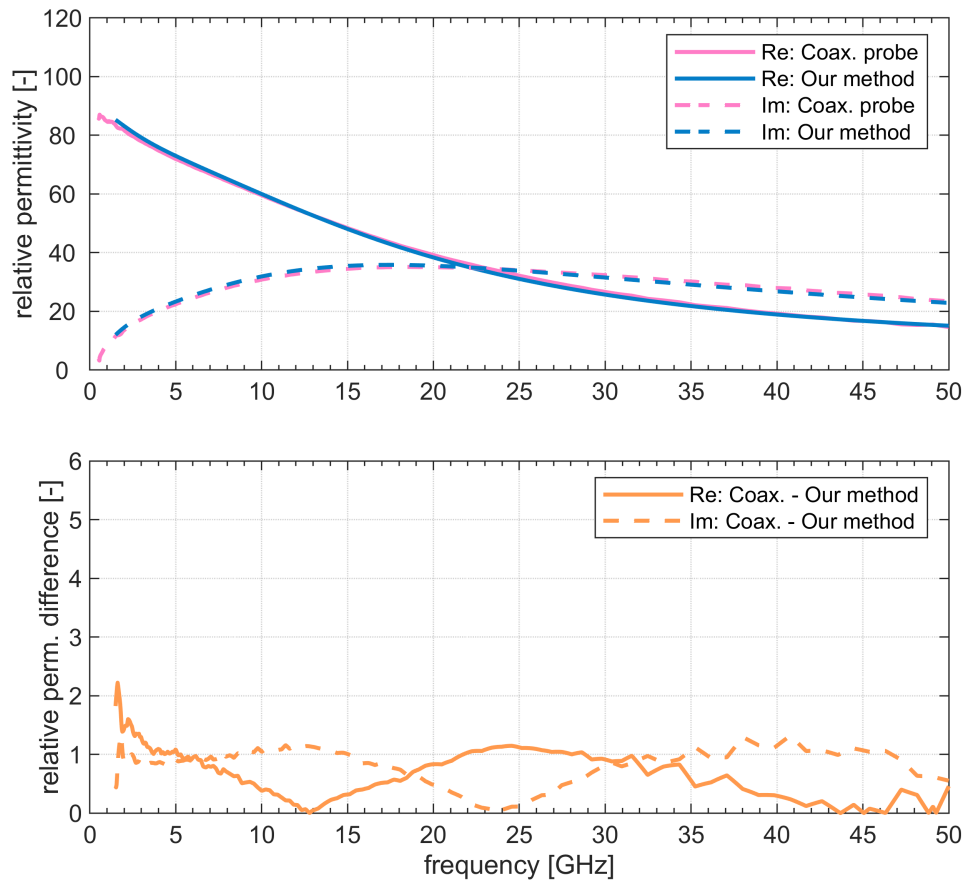
8.2.1 Concentrations 50 mg/mL

Figure 8.3: Comparison between complex permittivities obtained from the coaxial probe [3] and from our method – **MUT cysteine 50 mg/mL**.
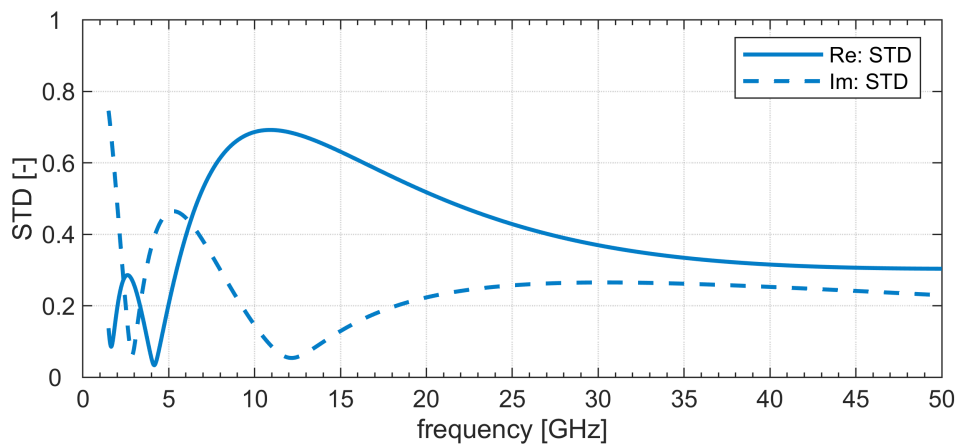

Figure 8.4: Standard deviation of complex permittivity from our method (five repetitions) – **MUT cysteine 50 mg/mL**.
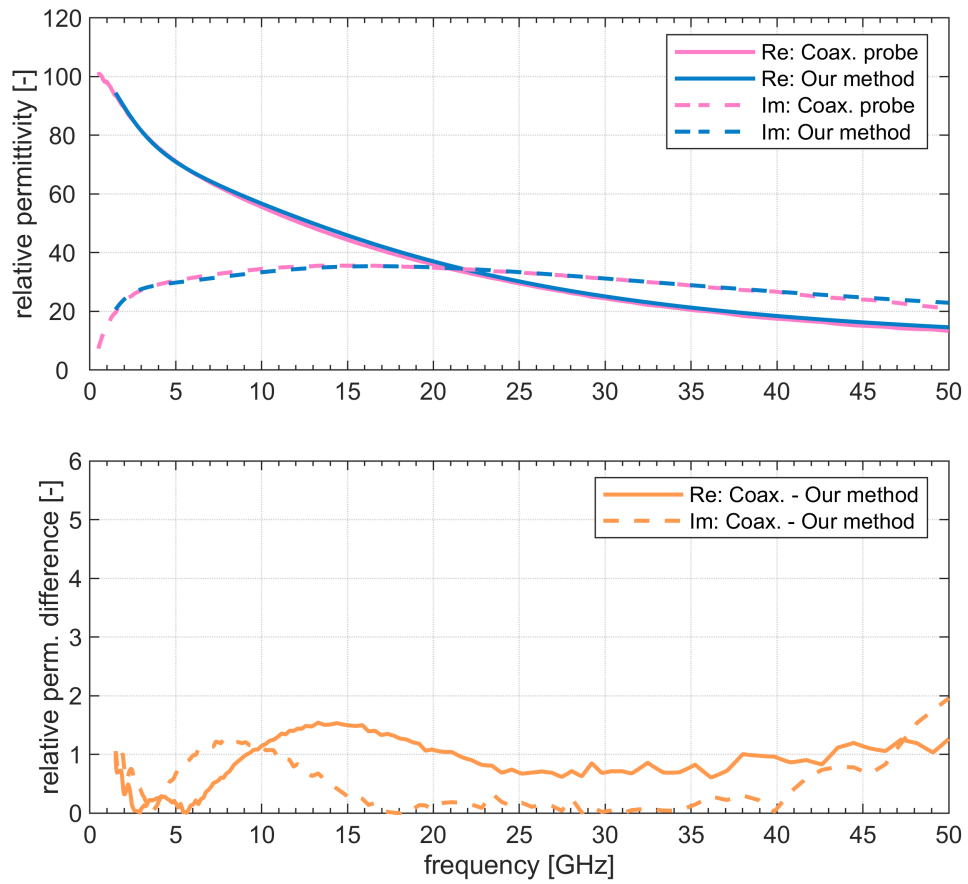
43

■ 8.2.2   Concentrations 100 mg/mL

Figure 8.5: Comparison between complex permittivities obtained from the coaxial probe [3] and from our method – **MUT alanine 100 mg/mL**.

Figure 8.6: Standard deviation of complex permittivity from our method (five repetitions) – **MUT alanine 100 mg/mL**.

Figure 8.7: Comparison between complex permittivities obtained from the coaxial probe [3] and from our method – **MUT cysteine 100 mg/mL**.

Figure 8.8: Standard deviation of complex permittivity from our method (five repetitions) – **MUT cysteine 100 mg/mL**.

8.2.3 Concentrations 150 mg/mL

Figure 8.9: Comparison between complex permittivities obtained from the coaxial probe [3] and from our method – **MUT alanine 150 mg/mL**.
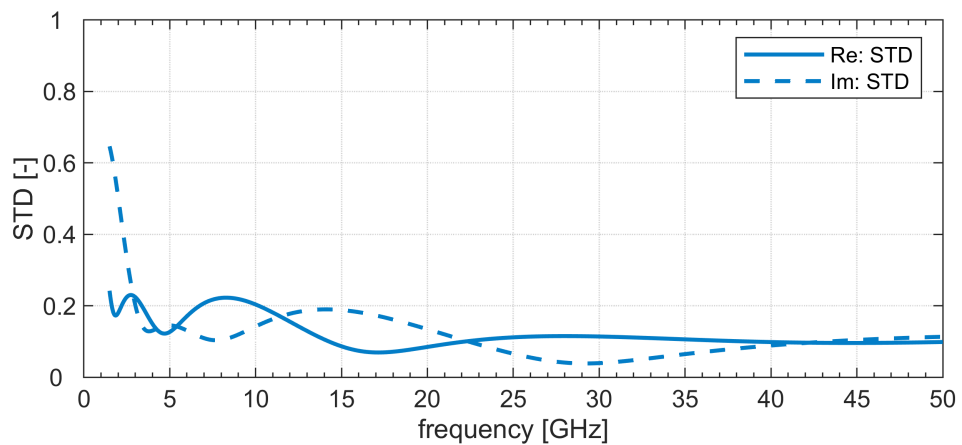

Figure 8.10: Standard deviation of complex permittivity from our method (five repetitions) – **MUT alanine 150 mg/mL**.
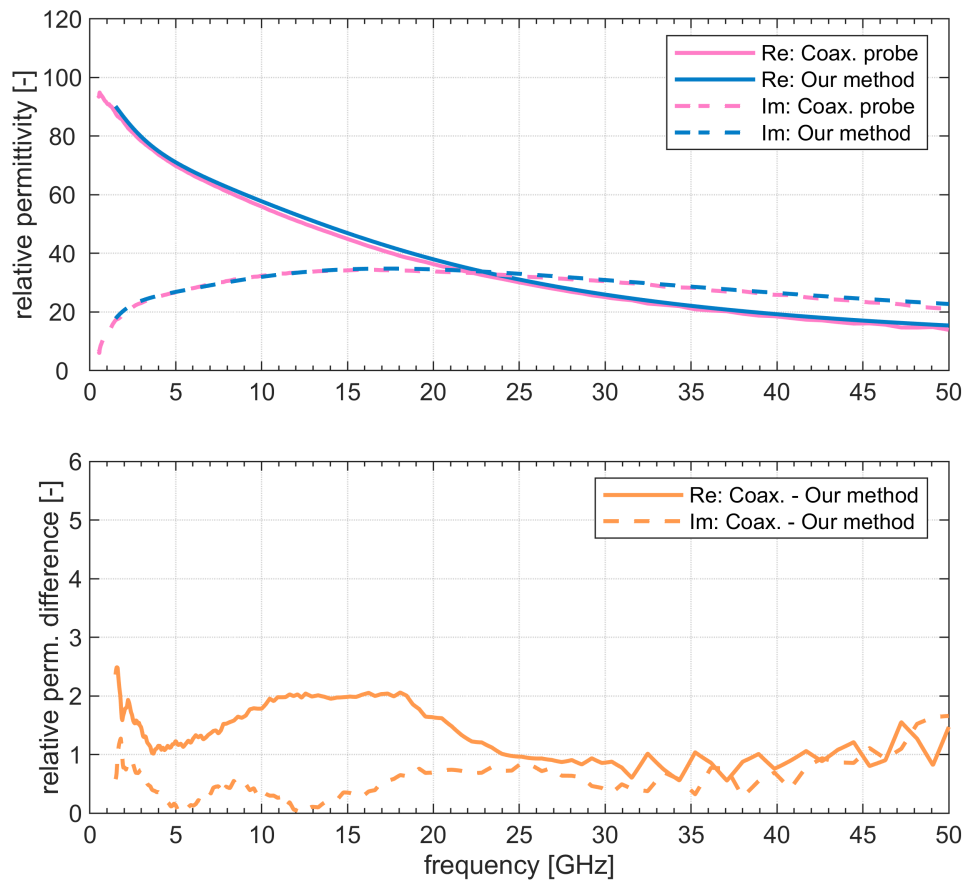
Figure 8.11: Comparison between complex permittivities obtained from the coaxial probe [3] and from our method – **MUT cysteine 150 mg/mL**.
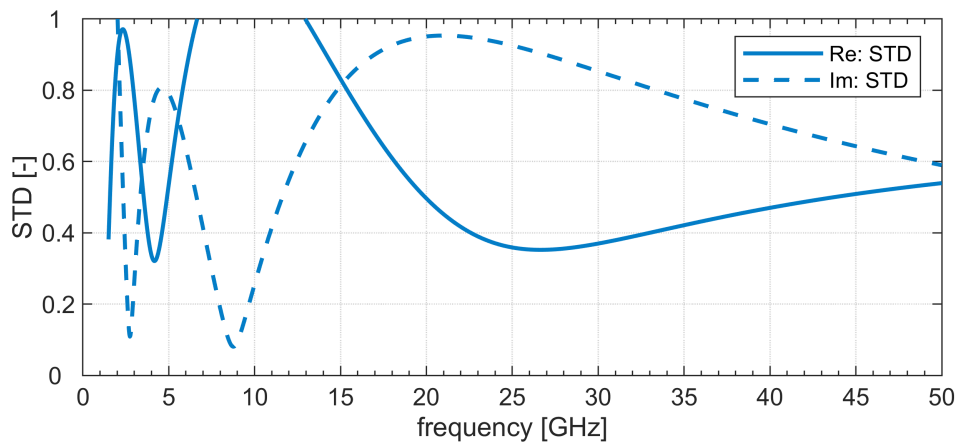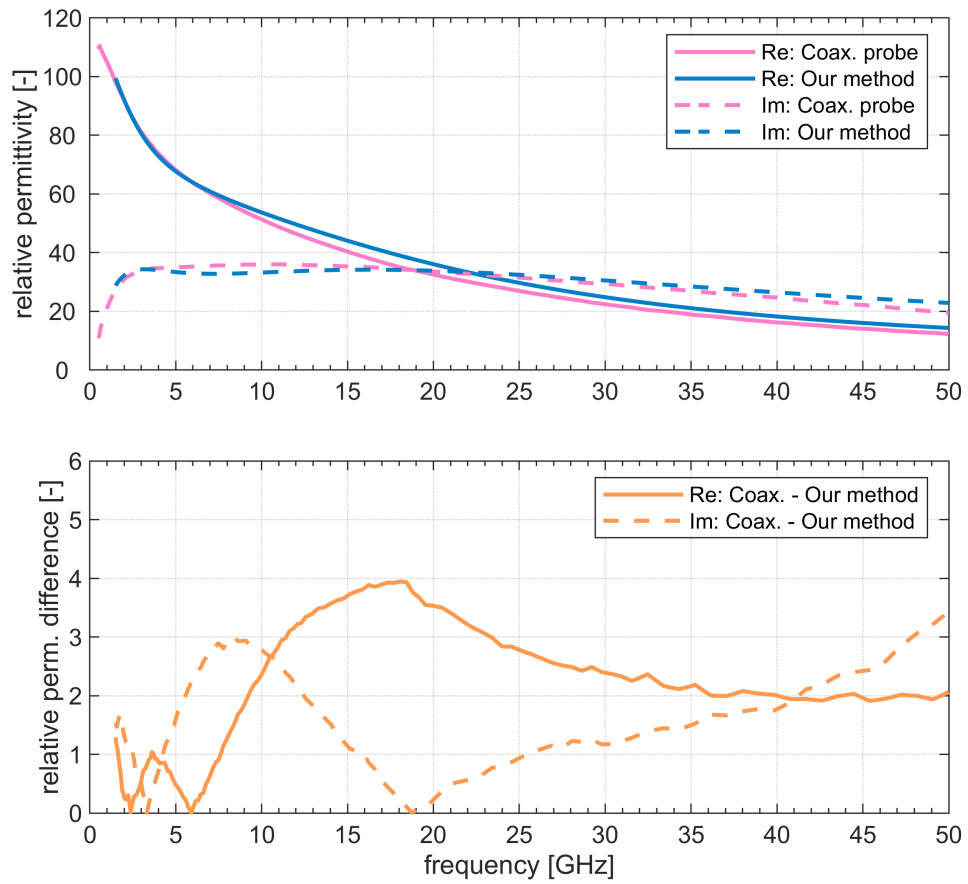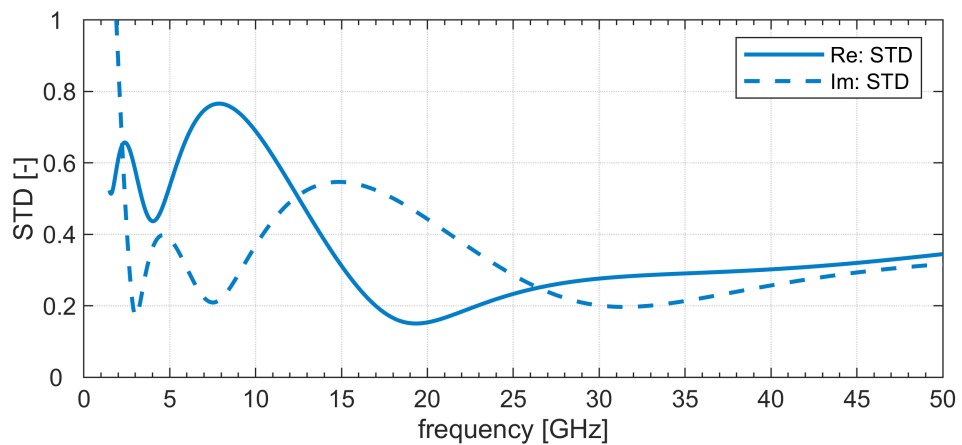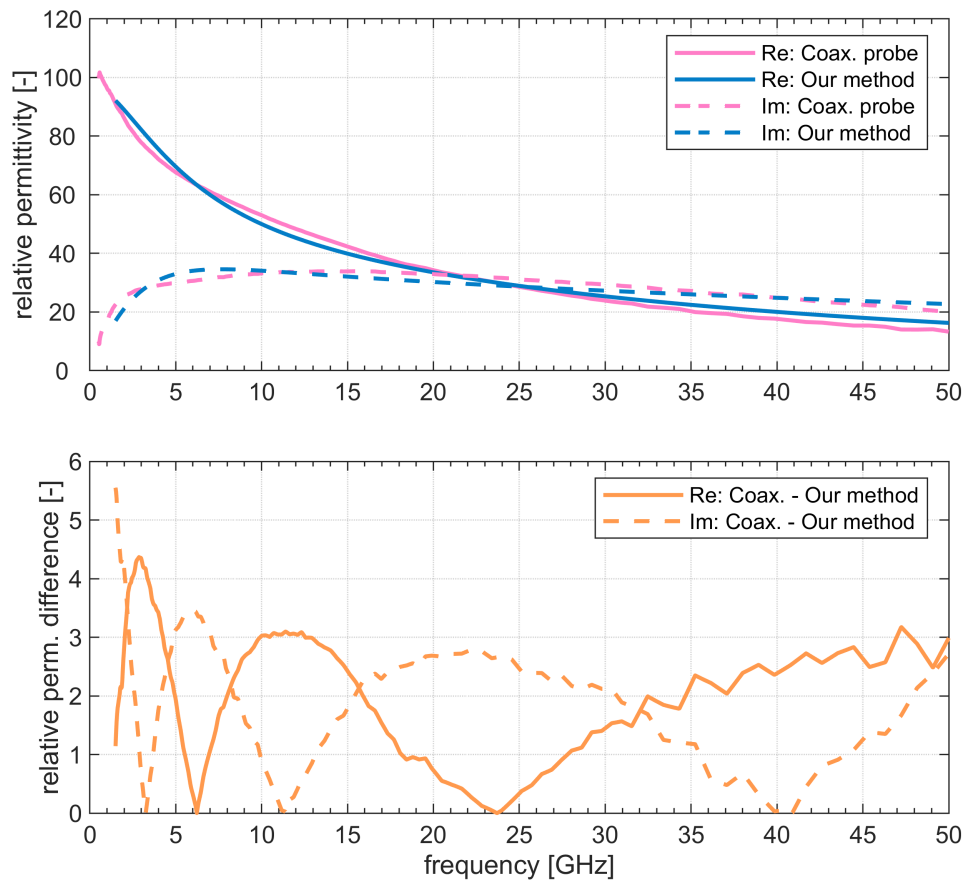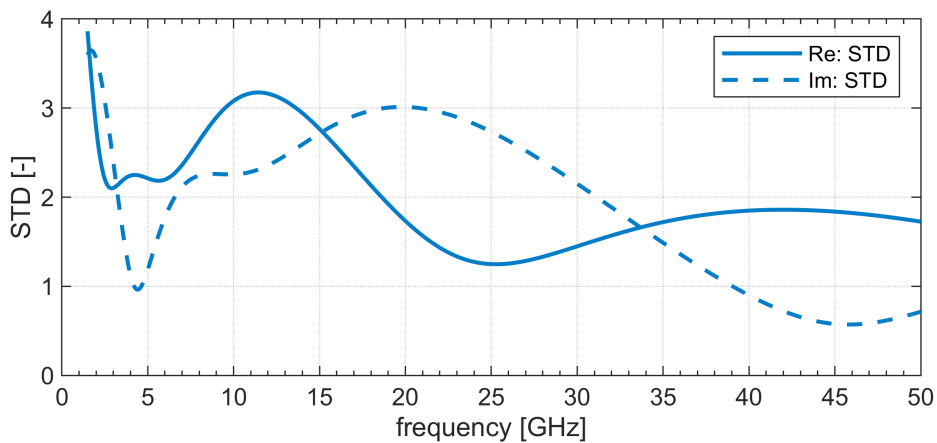

Figure 8.12: Standard deviation of complex permittivity from our method (five repetitions) – **MUT cysteine 150 mg/mL**.

47

■ 8.3 Evaluation of Results

We can see that our method works well. As expected, in the case of data from the simulator/reference measurement, the method almost overlaps the reference data.

In the case of real use, the method also works well. Quantitative results can be found in Tables 8.1 and 8.2 , where we can find the average and maximum deviation of our method from the reference measurement of permittivity by coaxial probe.

However, it must be said that the data from the coaxial probe were measured only at 201 frequency points. Our method works at 1601 points, and the data from the coaxial probe were therefore linearly interpolated for comparison purposes.

	mean deviation	maximum deviation
alanine 100 mg/mL	0.90 (2.57 %)	1.54
alanine 150 mg/mL	2.32 (7.07 %)	3.95
cysteine 50 mg/mL	0.62 (1.67 %)	2.22
cysteine 100 mg/mL	1.26 (3.57 %)	2.49
cysteine 150 mg/mL	1.96 (5.78 %)	4.37

Table 8.1: Absolute permittivity deviations of our method from the reference measurement – real components.

	mean deviation	maximum deviation
alanine 100 mg/mL	0.48 (1.60 %)	1.96
alanine 150 mg/mL	1.61 (5.40 %)	3.44
cysteine 50 mg/mL	0.82 (2.79 %)	1.32
cysteine 100 mg/mL	0.61 (3.11 %)	1.66
cysteine 150 mg/mL	1.75 (6.06 %)	5.56

Table 8.2: Absolute permittivity deviations of our method from the reference measurement – imaginary components.

As we can see, the farther we are from the permittivity of the calibration solutions, the worse the method works. For solutions with a concentration of 150 mg/mL, a large standard deviation begins to appear. This might be because, at such high concentrations, the sample placed on the transmission line tended to flow through the vias away. This caused differences in the measurement of the S–parameters.

■ 8.4 Discussion

Our method is a combination of the previous methods from Section 2.4 with several new elements. We can divide the method into two parts. In the first part, when the method is calibrated, we use real measured data and

data from the simulator. The uniqueness of this method is that the result of calibration is the so-called field shape factors (also called geometry factors), obtained from the derived analytical relations (see Section 5.1.2). These field shape factors capture the geometry of the electromagnetic field inside the sample. In the second part we obtain permittivity of the MUT from closed form equations. This is again unique because we have complex permittivity explicitly stated.

This method is therefore computationally fast, thanks to the Trace equation (see Section 2.4.2) immune to the influence of the imperfections leading to and from the MUT and accurate, even at the problematic low frequencies.

Our method is less accurate in the area where the Trace equation tends to break down. This is due to complex hyperbolic functions, when small numerical inaccuracies can multiply into huge values (see Section 6.2.1). The solution to this problem should be shorter CBCPW line. Another improvement could be the analytical rule for finding the area of the base solution of the γ from Section 6.2.2. The numerical solver then would not have to be iterated many times. It would only run once, when based on a correct estimate of the starting point, it would be possible to quickly converge to the correct solution. This would speed up the whole method even more.

Chapter **9**

Conclusion

In this work, the state of the art of broadband complex permittivity extraction was described in Section 2. The basic principles of the interaction of the electromagnetic field with matter in the radio frequency and microwave band were described in Section 3. In Section 5 special emphasis was placed on the broadband extraction of complex permittivity of materials with a focus on planar transmission lines, specifically the coplanar waveguide.

In Section 6 a semi-analytical method for extracting complex permittivity spectra from measured frequency-dependent S–parameters, was obtained. In Section 7, the S–parameters of the CBCPW lines with liquid samples of water and biomolecules were measured up to 50 GHz.

Finally, the method was tested in real life on the measured S–parameters. The extracted permittivity was compared with the reference data measured using a coaxial probe. The results of our method differed from the reference method on average by 1.41 (4.05 %) for the real component and by 1.05 (3.56 %) for the imaginary component of permittivity. The average is then considered from all MUT concentrations, even across the problematic concentrations of 150 mg/mL.

The CBCPW transmission line broadband permittivity extraction method could be used in the future for the development of a complex permittivity sensing device for general liquid samples.

Chapter 10

Annex

10.1 Assumptions:

From [22, eq. (1a, 1b, 2, 4)] and [24, eq. (79)]:

$$M_1 = X \cdot R_1^{Z_0, Z_0}(l_1) \cdot Y \tag{10.1}$$

$$M_2 = X \cdot R_2^{Z_0, Z_0}(l_2) \cdot Y \tag{10.2}$$

where:

$$R_1^{Z_0, Z_0}(l_1) = Q^{Z_0, Z_{c1}} \cdot R_1^{Z_{c1}, Z_{c1}}(l_1) \cdot Q^{Z_{c1}, Z_0} \tag{10.3}$$

where:

$$Q^{Z_n, Z_m} = \frac{1}{2Z_m} \left| \frac{Z_m}{Z_n} \right| \sqrt{\frac{\Re(Z_n)}{\Re(Z_m)}} \begin{bmatrix} Z_m + Z_n & Z_m - Z_n \\ Z_m - Z_n & Z_m + Z_n \end{bmatrix} \tag{10.4}$$

$$R_1^{Z_{c1}, Z_{c1}}(l_1) = \begin{bmatrix} e^{-\gamma_1 \cdot l_1} & 0 \\ 0 & e^{\gamma_1 \cdot l_1} \end{bmatrix} \tag{10.5}$$

10.2 Derivation if $Z_{c1} = Z_{c2}$

$$
\begin{aligned}
M_2 \cdot M_1^{-1} &= [X \cdot R_2^{Z_0, Z_0}(l_2) \cdot Y] \cdot [X \cdot R_1^{Z_0, Z_0}(l_1) \cdot Y]^{-1} =^1= \\
&\quad X \cdot R_2^{Z_0, Z_0}(l_2) \cdot Y \cdot Y^{-1} \cdot [R_1^{Z_0, Z_0}(l_1)]^{-1} \cdot X^{-1} = \\
&\qquad X \cdot R_2^{Z_0, Z_0}(l_2) \cdot [R_1^{Z_0, Z_0}(l_1)]^{-1} \cdot X^{-1} \quad (10.6)
\end{aligned}
$$

$$
\begin{aligned}
\text{Tr}\left\{ M_2 \cdot M_1^{-1} \right\} =^2= \text{Tr}\left\{ R_2^{Z_0, Z_0}(l_2) \cdot [R_1^{Z_0, Z_0}(l_1)]^{-1} \cdot X^{-1} \cdot X \right\} = \\
\text{Tr}\left\{ R_2^{Z_0, Z_0}(l_2) \cdot [R_1^{Z_0, Z_0}(l_1)]^{-1} \right\} \quad (10.7)
\end{aligned}
$$

See eq. (10.3) and eq. (10.5).

$$M_1^{-1} \Rightarrow [R_1^{Z_0,Z_0}(l_1)]^{-1} =$$
$$[Q^{Z_0,Z_{c1}} \cdot R_1^{Z_{c1},Z_{c1}}(l_1) \cdot Q^{Z_{c1},Z_0}]^{-1} =^1=$$
$$[Q^{Z_{c1},Z_0}]^{-1} \cdot \begin{bmatrix} e^{-\gamma_1 \cdot l_1} & 0 \\ 0 & e^{\gamma_1 \cdot l_1} \end{bmatrix}^{-1} \cdot [Q^{Z_0,Z_{c1}}]^{-1} =$$
$$Q^{Z_0,Z_{c1}} \cdot \begin{bmatrix} e^{\gamma_1 \cdot l_1} & 0 \\ 0 & e^{-\gamma_1 \cdot l_1} \end{bmatrix} \cdot Q^{Z_{c1},Z_0} =$$
$$Q^{Z_0,Z_{c1}} \cdot R_1^{Z_{c1},Z_{c1}}(-l_1) \cdot Q^{Z_{c1},Z_0} =$$
$$Q^{Z_0,Z_{c1}} \cdot Q^{Z_{c1},Z_{c2}} \cdot R_1^{Z_{c2},Z_{c2}}(-l_1) \cdot Q^{Z_{c2},Z_{c1}} \cdot Q^{Z_{c1},Z_0} =$$
$$Q^{Z_0,Z_{c2}} \cdot R_1^{Z_{c2},Z_{c2}}(-l_1) \cdot Q^{Z_{c2},Z_0} \quad (10.8)$$

$$M_2 \cdot M_1^{-1} = R_2^{Z_0,Z_0}(l_2) \cdot [R_1^{Z_0,Z_0}(l_1)]^{-1} =$$
$$Q^{Z_0,Z_{c2}} \cdot R_2^{Z_{c2},Z_{c2}}(l_2) \cdot Q^{Z_{c2},Z_0} \cdot Q^{Z_0,Z_{c2}} \cdot R_1^{Z_{c2},Z_{c2}}(-l_1) \cdot Q^{Z_{c2},Z_0} =$$
$$Q^{Z_0,Z_{c2}} \cdot R_2^{Z_{c2},Z_{c2}}(l_2) \cdot R_1^{Z_{c2},Z_{c2}}(-l_1) \cdot Q^{Z_{c2},Z_0} \quad (10.9)$$

$$\text{Tr}\left\{M_2 \cdot M_1^{-1}\right\} =^2=$$
$$\text{Tr}\left\{R_2^{Z_{c2},Z_{c2}}(l_2) \cdot R_1^{Z_{c2},Z_{c2}}(-l_1) \cdot Q^{Z_{c2},Z_0} \cdot Q^{Z_0,Z_{c2}}\right\} =$$
$$\text{Tr}\left\{R_2^{Z_{c2},Z_{c2}}(l_2) \cdot R_1^{Z_{c2},Z_{c2}}(-l_1)\right\} \quad (10.10)$$

$$\text{Tr}\left\{M_2 \cdot M_1^{-1}\right\} = \text{Tr}\left\{ \begin{bmatrix} e^{-\gamma_2 \cdot l_2} & 0 \\ 0 & e^{\gamma_2 \cdot l_2} \end{bmatrix} \cdot \begin{bmatrix} e^{\gamma_1 \cdot l_1} & 0 \\ 0 & e^{-\gamma_1 \cdot l_1} \end{bmatrix} \right\} =$$
$$\text{Tr}\left\{ \begin{bmatrix} e^{-\gamma_2 \cdot l_2} \cdot e^{\gamma_1 \cdot l_1} & 0 \\ 0 & e^{\gamma_2 \cdot l_2} \cdot e^{-\gamma_1 \cdot l_1} \end{bmatrix} \right\} = e^{-\gamma_2 \cdot l_2} \cdot e^{\gamma_1 \cdot l_1} + e^{\gamma_2 \cdot l_2} \cdot e^{-\gamma_1 \cdot l_1} =$$
$$e^{\gamma_1 \cdot l_1 - \gamma_2 \cdot l_2} + e^{\gamma_2 \cdot l_2 - \gamma_1 \cdot l_1} = \frac{2 \cdot e^{\gamma_1 \cdot l_1 - \gamma_2 \cdot l_2} + 2 \cdot e^{-(\gamma_1 \cdot l_1 - \gamma_2 \cdot l_2)}}{2} =^3=$$
$$2 \cdot \cosh\left(\gamma_1 \cdot l_1 - \gamma_2 \cdot l_2\right) =^4=$$
$$2\cosh\left(\gamma_1 \cdot l_1\right)\cosh\left(\gamma_2 \cdot l_2\right) - 2\sinh\left(\gamma_1 \cdot l_1\right)\sinh\left(\gamma_2 \cdot l_2\right) \quad (10.11)$$

10.3 Derivation if $Z_{c1} \neq Z_{c2}$

Rewritten eq. (10.8):

$$M_1^{-1} \Rightarrow [R_1^{Z_0,Z_0}(l_1)]^{-1} =$$
$$[Q^{Z_0,Z_{c1}} \cdot R_1^{Z_{c1},Z_{c1}}(l_1) \cdot Q^{Z_{c1},Z_0}]^{-1} =^1=$$
$$[Q^{Z_{c1},Z_0}]^{-1} \cdot \begin{bmatrix} e^{-\gamma_1 \cdot l_1} & 0 \\ 0 & e^{\gamma_1 \cdot l_1} \end{bmatrix}^{-1} \cdot [Q^{Z_0,Z_{c1}}]^{-1} =$$
$$Q^{Z_0,Z_{c1}} \cdot \begin{bmatrix} e^{\gamma_1 \cdot l_1} & 0 \\ 0 & e^{-\gamma_1 \cdot l_1} \end{bmatrix} \cdot Q^{Z_{c1},Z_0} =$$
$$Q^{Z_0,Z_{c1}} \cdot R_1^{Z_{c1},Z_{c1}}(-l_1) \cdot Q^{Z_{c1},Z_0} \quad (10.12)$$

$$M_2 \cdot M_1^{-1} = R_2^{Z_0,Z_0}(l_2) \cdot [R_1^{Z_0,Z_0}(l_1)]^{-1} =$$
$$Q^{Z_0,Z_{c2}} \cdot R_2^{Z_{c2},Z_{c2}}(l_2) \cdot Q^{Z_{c2},Z_0} \cdot Q^{Z_0,Z_{c1}} \cdot R_1^{Z_{c1},Z_{c1}}(-l_1) \cdot Q^{Z_{c1},Z_0} =$$
$$Q^{Z_0,Z_{c2}} \cdot R_2^{Z_{c2},Z_{c2}}(l_2) \cdot Q^{Z_{c2},Z_{c1}} \cdot R_1^{Z_{c1},Z_{c1}}(-l_1) \cdot Q^{Z_{c1},Z_0} \quad (10.13)$$

$$\text{Tr}\left\{M_2 \cdot M_1^{-1}\right\} =^2=$$
$$\text{Tr}\left\{R_2^{Z_{c2},Z_{c2}}(l_2) \cdot Q^{Z_{c2},Z_{c1}} \cdot R_1^{Z_{c1},Z_{c1}}(-l_1) \cdot Q^{Z_{c1},Z_0} \cdot Q^{Z_0,Z_{c2}}\right\} =$$
$$\text{Tr}\left\{R_2^{Z_{c2},Z_{c2}}(l_2) \cdot Q^{Z_{c2},Z_{c1}} \cdot R_1^{Z_{c1},Z_{c1}}(-l_1) \cdot Q^{Z_{c1},Z_{c2}}\right\} =$$
$$\text{Tr}\left\{\begin{bmatrix} e^{-\gamma_2 \cdot l_2} & 0 \\ 0 & e^{\gamma_2 \cdot l_2} \end{bmatrix} \cdot \frac{1}{2Z_{c1}}\left|\frac{Z_{c1}}{Z_{c2}}\right|\sqrt{\frac{\Re(Z_{c2})}{\Re(Z_{c1})}} \begin{bmatrix} Z_{c1}+Z_{c2} & Z_{c1}-Z_{c2} \\ Z_{c1}-Z_{c2} & Z_{c1}+Z_{c2} \end{bmatrix} \cdot \right.$$
$$\left. \begin{bmatrix} e^{\gamma_1 \cdot l_1} & 0 \\ 0 & e^{-\gamma_1 \cdot l_1} \end{bmatrix} \cdot \frac{1}{2Z_{c2}}\left|\frac{Z_{c2}}{Z_{c1}}\right|\sqrt{\frac{\Re(Z_{c1})}{\Re(Z_{c2})}} \begin{bmatrix} Z_{c2}+Z_{c1} & Z_{c2}-Z_{c1} \\ Z_{c2}-Z_{c1} & Z_{c2}+Z_{c1} \end{bmatrix}\right\} \quad (10.14)$$

$$\text{Tr}\left\{M_2 \cdot M_1^{-1}\right\} =^5=$$
$$\frac{1}{2Z_{c1}}\left|\frac{Z_{c1}}{Z_{c2}}\right|\sqrt{\frac{\Re(Z_{c2})}{\Re(Z_{c1})}} \cdot \frac{1}{2Z_{c2}}\left|\frac{Z_{c2}}{Z_{c1}}\right|\sqrt{\frac{\Re(Z_{c1})}{\Re(Z_{c2})}} \cdot \text{Tr}\left\{\begin{bmatrix} e^{-\gamma_2 \cdot l_2} & 0 \\ 0 & e^{\gamma_2 \cdot l_2} \end{bmatrix} \cdot \right.$$
$$\left. \begin{bmatrix} Z_{c1}+Z_{c2} & Z_{c1}-Z_{c2} \\ Z_{c1}-Z_{c2} & Z_{c1}+Z_{c2} \end{bmatrix} \cdot \begin{bmatrix} e^{\gamma_1 \cdot l_1} & 0 \\ 0 & e^{-\gamma_1 \cdot l_1} \end{bmatrix} \cdot \begin{bmatrix} Z_{c2}+Z_{c1} & Z_{c2}-Z_{c1} \\ Z_{c2}-Z_{c1} & Z_{c2}+Z_{c1} \end{bmatrix}\right\} =^{6,7,8}=$$
$$\frac{1}{2Z_{c1}} \cdot \frac{1}{2Z_{c2}} \cdot \text{Tr}\left\{\begin{bmatrix} e^{-\gamma_2 \cdot l_2} \cdot (Z_{c1}+Z_{c2}) & e^{-\gamma_2 \cdot l_2} \cdot (Z_{c1}-Z_{c2}) \\ e^{\gamma_2 \cdot l_2} \cdot (Z_{c1}-Z_{c2}) & e^{\gamma_2 \cdot l_2} \cdot (Z_{c1}+Z_{c2}) \end{bmatrix} \cdot \right.$$
$$\left. \begin{bmatrix} e^{\gamma_1 \cdot l_1} \cdot (Z_{c2}+Z_{c1}) & e^{\gamma_1 \cdot l_1} \cdot (Z_{c2}-Z_{c1}) \\ e^{-\gamma_1 \cdot l_1} \cdot (Z_{c2}-Z_{c1}) & e^{-\gamma_1 \cdot l_1} \cdot (Z_{c2}+Z_{c1}) \end{bmatrix}\right\} =$$
$$\frac{1}{4Z_{c1}Z_{c2}} \cdot \text{Tr}\left\{\begin{bmatrix} a & x_1 \\ x_2 & b \end{bmatrix}\right\} \quad (10.15)$$

55

$$a = e^{\gamma_1 \cdot l_1 - \gamma_2 \cdot l_2} \cdot (Z_{c1} + Z_{c2})^2 - e^{-\gamma_1 \cdot l_1 - \gamma_2 \cdot l_2} \cdot (Z_{c1} - Z_{c2})^2 \qquad (10.16)$$

$$b = e^{\gamma_2 \cdot l_2 - \gamma_1 \cdot l_1}(Z_{c1} + Z_{c2})^2 - e^{\gamma_1 \cdot l_1 + \gamma_2 \cdot l_2} \cdot (Z_{c1} - Z_{c2})^2 \qquad (10.17)$$

$$\mathrm{Tr}\left\{M_2 \cdot M_1^{-1}\right\} = \frac{1}{4Z_{c1}Z_{c2}} \cdot (a + b) =$$

$$\frac{1}{4Z_{c1}Z_{c2}} \cdot [e^{\gamma_1 \cdot l_1 - \gamma_2 \cdot l_2} \cdot (Z_{c1} + Z_{c2})^2 - e^{-\gamma_1 \cdot l_1 - \gamma_2 \cdot l_2} \cdot (Z_{c1} - Z_{c2})^2 +$$

$$e^{\gamma_2 \cdot l_2 - \gamma_1 \cdot l_1} \cdot (Z_{c1} + Z_{c2})^2 - e^{\gamma_1 \cdot l_1 + \gamma_2 \cdot l_2} \cdot (Z_{c1} - Z_{c2})^2] =$$

$$\frac{1}{4Z_{c1}Z_{c2}} \cdot [(e^{\gamma_1 \cdot l_1 - \gamma_2 \cdot l_2} + e^{\gamma_2 \cdot l_2 - \gamma_1 \cdot l_1}) \cdot (Z_{c1} + Z_{c2})^2$$

$$- (e^{-\gamma_1 \cdot l_1 - \gamma_2 \cdot l_2} + e^{\gamma_1 \cdot l_1 + \gamma_2 \cdot l_2}) \cdot (Z_{c1} - Z_{c2})^2 =^3=$$

$$\frac{1}{2Z_{c1}Z_{c2}} \cdot [(\cosh{(\gamma_1 \cdot l_1 - \gamma_2 \cdot l_2)} \cdot (Z_{c1} + Z_{c2})^2 - \cosh{(\gamma_1 \cdot l_1 + \gamma_2 \cdot l_2)} \cdot (Z_{c1} - Z_{c2})^2] =^4=$$

$$\frac{1}{2Z_{c1}Z_{c2}} \cdot \left\{ [\cosh{(\gamma_1 \cdot l_1)}\cosh{(\gamma_2 \cdot l_2)} - \sinh{(\gamma_1 \cdot l_1)}\sinh{(\gamma_2 \cdot l_2)}] \cdot (Z_{c1} + Z_{c2})^2 \right.$$

$$\left. - [\cosh{(\gamma_1 \cdot l_1)}\cosh{(\gamma_2 \cdot l_2)} + \sinh{(\gamma_1 \cdot l_1)}\sinh{(\gamma_2 \cdot l_2)}] \cdot (Z_{c1} - Z_{c2})^2 \right\} =$$

$$\frac{1}{2Z_{c1}Z_{c2}} \cdot \left\{ \cosh{(\gamma_1 \cdot l_1)}\cosh{(\gamma_2 \cdot l_2)} \cdot (Z_{c1} + Z_{c2})^2 - \sinh{(\gamma_1 \cdot l_1)}\sinh{(\gamma_2 \cdot l_2)} \cdot (Z_{c1} + Z_{c2})^2 \right.$$

$$\left. - \cosh{(\gamma_1 \cdot l_1)}\cosh{(\gamma_2 \cdot l_2)} \cdot (Z_{c1} - Z_{c2})^2 - \sinh{(\gamma_1 \cdot l_1)}\sinh{(\gamma_2 \cdot l_2)} \cdot (Z_{c1} - Z_{c2})^2 \right\} =$$

$$\frac{1}{2Z_{c1}Z_{c2}} \cdot \left\{ \cosh{(\gamma_1 \cdot l_1)}\cosh{(\gamma_2 \cdot l_2)} \cdot [(Z_{c1} + Z_{c2})^2 - (Z_{c1} - Z_{c2})^2] \right.$$

$$\left. - \sinh{(\gamma_1 \cdot l_1)}\sinh{(\gamma_2 \cdot l_2)} \cdot [(Z_{c1} + Z_{c2})^2 + (Z_{c1} - Z_{c2})^2] \right\} =$$

$$\frac{1}{2Z_{c1}Z_{c2}} \cdot \left\{ \cosh{(\gamma_1 \cdot l_1)}\cosh{(\gamma_2 \cdot l_2)} \cdot (4Z_{c1}Z_{c2}) \right.$$

$$\left. - \sinh{(\gamma_1 \cdot l_1)}\sinh{(\gamma_2 \cdot l_2)} \cdot (2Z_{c1}^2 + 2Z_{c2}^2) \right\} =$$

$$2 \cdot \cosh{(\gamma_1 \cdot l_1)}\cosh{(\gamma_2 \cdot l_2)} - \left(\frac{Z_{c1}}{Z_{c2}} + \frac{Z_{c2}}{Z_{c1}}\right) \cdot \sinh{(\gamma_1 \cdot l_1)}\sinh{(\gamma_2 \cdot l_2)}$$

$$(10.18)$$

$$\mathrm{Tr}\left\{M_2 \cdot M_1^{-1}\right\} =$$

$$2 \cdot \cosh{(\gamma_1 \cdot l_1)}\cosh{(\gamma_2 \cdot l_2)} - \left(\frac{Z_{c1}}{Z_{c2}} + \frac{Z_{c2}}{Z_{c1}}\right) \cdot \sinh{(\gamma_1 \cdot l_1)}\sinh{(\gamma_2 \cdot l_2)}$$

$$(10.19)$$

$(^1)$ $[A \cdot B \cdot C]^{-1} = C^{-1} \cdot B^{-1} \cdot A^{-1}$

$(^2)$ $\text{Tr}[A \cdot B \cdot C] = \text{Tr}[B \cdot C \cdot A]$

$(^3)$ $\cosh(x) = \dfrac{e^x + e^{-x}}{2}$

$(^4)$ $\cosh(x \pm y) = \cosh(x)\cosh(y) \pm \sinh(x)\sinh(y)$

$(^5)$ $\text{Tr}[k \cdot A] = k \cdot \text{Tr}[A]$

$(^6)$ $\sqrt{a \cdot b} = \sqrt{a} \cdot \sqrt{b}$

$(^7)$ $\left| \dfrac{a}{b} \right| = \dfrac{|a|}{|b|}$

$(^8)$ $[A \cdot B] \cdot C = A \cdot [B \cdot C]$

Bibliography

[1] W. Ellison, "Permittivity of pure water, at standard atmospheric pressure, over the frequency range 0–25 thz and the temperature range 0–100 c," *Journal of physical and chemical reference data*, vol. 36, no. 1, pp. 1–18, 2007.

[2] N. E. Hill, "Dielectric behaviour of biological molecules in solution by eh grant, rj sheppard and sp south. pp. 237. clarendon press: Oxford university press, oxford and london. 1978. in the series monographs on physical biochemistry.£ 11.00," 1979.

[3] D. Havelka, O. Krivosudský, J. Průša, and M. Cifra, "Rational design of sensor for broadband dielectric spectroscopy of biomolecules," *Sensors and Actuators B: Chemical*, vol. 273, pp. 62–69, 2018.

[4] M. Cifra, J. Průša, D. Havelka, and O. Krivosudský, "Water models in molecular dynamics simulation prediction of dielectric properties of biomaterials," *IEEE Journal of Electromagnetics, RF and Microwaves in Medicine and Biology*, vol. 3, no. 2, pp. 97–104, 2019.

[5] "Microwave Dielectric Spectroscopy Workshop." `http://academy.cba.mit.edu/classes/input_devices/DS.pdf`. Date: 2022-05-14.

[6] V. Raicu and Y. Feldman, *Dielectric relaxation in biological systems: Physical principles, methods, and applications.* Oxford University Press, USA, 2015.

[7] K. Grenier, D. Dubuc, P.-E. Poleni, M. Kumemura, H. Toshiyoshi, T. Fujii, and H. Fujita, "Integrated broadband microwave and microfluidic sensor dedicated to bioengineering," *IEEE Transactions on microwave theory and techniques*, vol. 57, no. 12, pp. 3246–3253, 2009.

[8] J. C. Booth, N. D. Orloff, J. Mateu, M. Janezic, M. Rinehart, and J. A. Beall, "Quantitative permittivity measurements of nanoliter liquid volumes in microfluidic channels to 40 ghz," *IEEE Transactions on Instrumentation and Measurement*, vol. 59, no. 12, pp. 3279–3288, 2010.

[9] O. Krivosudskỳ, D. Havelka, D. E. Chafai, and M. Cifra, "Microfluidic on-chip microwave sensing of the self-assembly state of tubulin," *Sensors and Actuators B: Chemical*, vol. 328, p. 129068, 2021.

[10] C. D. Abeyrathne, D. H. Huynh, T. T. Lee, T. C. Nguyen, B. Nasr, G. Chana, and E. Skafidas, "Gfap antibody detection using interdigital coplanar waveguide immunosensor," *IEEE Sensors Journal*, vol. 16, no. 9, pp. 2898–2905, 2016.

[11] A. C. Stelson, M. Liu, C. A. Little, C. J. Long, N. D. Orloff, N. Stephanopoulos, and J. C. Booth, "Label-free detection of conformational changes in switchable dna nanostructures with microwave microfluidics," *Nature communications*, vol. 10, no. 1, pp. 1–9, 2019.

[12] G. Guarin, M. Hofmann, J. Nehring, R. Weigel, G. Fischer, and D. Kissinger, "Miniature microwave biosensors: Noninvasive applications," *IEEE Microwave Magazine*, vol. 16, no. 4, pp. 71–86, 2015.

[13] S. Liu, N. D. Orloff, C. A. Little, W. Zhao, J. C. Booth, D. F. Williams, I. Ocket, D. M.-P. Schreurs, and B. Nauwelaers, "Hybrid characterization of nanolitre dielectric fluids in a single microfluidic channel up to 110 ghz," *IEEE Transactions on Microwave Theory and Techniques*, vol. 65, no. 12, pp. 5063–5073, 2017.

[14] X. Ma, N. D. Orloff, C. A. Little, C. J. Long, I. E. Hanemann, S. Liu, J. Mateu, J. C. Booth, and J. C. Hwang, "A multistate single-connection calibration for microwave microfluidics," *IEEE Transactions on Microwave Theory and Techniques*, vol. 66, no. 2, pp. 1099–1107, 2017.

[15] J. C. Booth, J. Mateu, M. Janezic, J. Baker-Jarvis, and J. A. Beall, "Broadband permittivity measurements of liquid and biological samples using microfluidic channels," in *2006 IEEE MTT-S International Microwave Symposium Digest*, pp. 1750–1753, IEEE, 2006.

[16] N. Meyne, W. Müller-Wichards, H. K. Trieu, and A. F. Jacob, "Quasi-lumped coplanar transmission-line sensors for broadband liquid characterization," in *2014 44th European Microwave Conference*, pp. 687–690, IEEE, 2014.

[17] D. Zhao, G. Rietveld, and G. M. Teunisse, "A multistep approach for accurate permittivity measurements of liquids using a transmission line method," *IEEE Transactions on Instrumentation and Measurement*, vol. 60, no. 7, pp. 2267–2274, 2010.

[18] D. Ye, M. S. Islam, G. Yu, and P. Wang, "A single-line single-channel method with closed-form formulas for the characterization of dielectric liquids," *IEEE Transactions on Microwave Theory and Techniques*, vol. 67, no. 6, pp. 2443–2450, 2019.

[19] B. Kang, J. Cho, C. Cheon, and Y. Kwon, "Nondestructive measurement of complex permittivity and permeability using multilayered coplanar waveguide structures," *IEEE Microwave and wireless components letters*, vol. 15, no. 5, pp. 381–383, 2005.

[20] M. D. Janezic and J. A. Jargon, "Complex permittivity determination from propagation constant measurements," *IEEE microwave and guided wave letters*, vol. 9, no. 2, pp. 76–78, 1999.

[21] J. Mateu, N. Orloff, M. Rinehart, and J. C. Booth, "Broadband permittivity of liquids extracted from transmission line measurements of microfluidic channels," in *2007 IEEE/MTT-S International Microwave Symposium*, pp. 523–526, IEEE, 2007.

[22] X. Bao, S. Liu, I. Ocket, J. Bao, D. Schreurs, S. Zhang, C. Cheng, K. Feng, and B. Nauwelaers, "A general line–line method for dielectric material characterization using conductors with the same cross-sectional geometry," *IEEE Microwave and Wireless Components Letters*, vol. 28, no. 4, pp. 356–358, 2018.

[23] N. J. Farcich, J. Salonen, and P. M. Asbeck, "Single-length method used to determine the dielectric constant of polydimethylsiloxane," *IEEE Transactions on Microwave Theory and techniques*, vol. 56, no. 12, pp. 2963–2971, 2008.

[24] R. B. Marks and D. F. Williams, "A general waveguide circuit theory," *Journal of research of the National Institute of Standards and Technology*, vol. 97, no. 5, p. 533, 1992.

[25] D. A. Frickey, "Conversions between s, z, y, h, abcd, and t parameters which are valid for complex source and load impedances," *IEEE Transactions on microwave theory and techniques*, vol. 42, no. 2, pp. 205–211, 1994.

[26] J. Zhang, M. Koledintseva, G. Antonini, J. Drewniak, A. Orlandi, and K. Rozanov, "Planar transmission line method for characterization of printed circuit board dielectrics," *Progress In Electromagnetics Research*, vol. 102, pp. 267–286, 2010.